FINAL REPORT

SAR Image Processing for Tracking, Display and Prediction of Sea Ice Dynamics

Prof. John F. Vesecky (Research)

Office of Naval Research Contract
N00014-85-K-0311

SPACE, TELECOMMUNICATIONS and RADIOSCIENCE LABORATORY

DEPARTMENT OF ELECTRICAL ENGINEERING, STARLAB / SEL
STANFORD UNIVERSITY • STANFORD, CALIFORNIA 94305-4055

FINAL REPORT

SAR Image Processing for Tracking, Display and Prediction of Sea Ice Dynamics

Prof. John F. Vesecky (Research)

Office of Naval Research Contract
N00014-85-K-0311

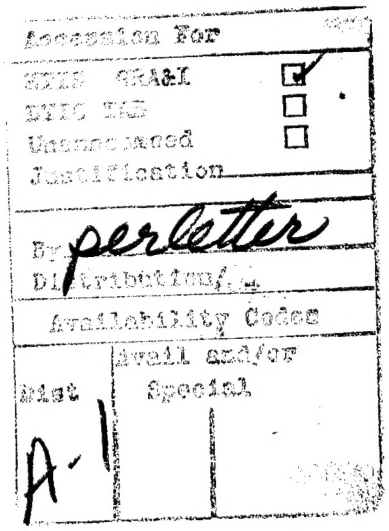

August, 1993

STAR LABORATORY
ELECTRICAL ENGINEERING DEPARTMENT
STANFORD UNIVERSITY

Stanford CA 94305

ABSTRACT

Sea ice is of fundamental importance in weather, climate and other geophysical processes. It is also an important factor for naval operations in the polar regions, in particular regarding transport of personnel and material in regions where sea ice is likely to be found and assessment and prediction of acoustic environments in polar regions. Because sea ice has a large geographic extent and short time scale for variability synthetic aperture radar (SAR) is a valuable technique in studying sea ice, particularly since images can be collected through clouds and at night. SAR information on sea ice will be available from several satellites in the 1990's (ERS-1, JERS-1, Almaz, Radarsat and possibly an EOS SAR). Automated interpretation techniques are required because of the large number and high information content of the SAR images becoming available. Here we report research on automated-computer-based techniques for such interpretation. The general problem that we face is to extract geophysical information from one or more SAR images. The work reported here concerns estimation of sea ice motion. Hence, we collect two images of a given geographical area some several days apart and note the change in sea ice location which gives us the average sea ice velocity vector. While one can do this manually by establishing tie points on the same piece of ice in the two scenes, an automated algorithm is preferable for both cost and consistency reasons. The research reported here covers the image pyramid area correlation (IPAC) and feature tracking algorithms. These two algorithms, when used together, can provide robust ice velocity estimates for ice that translates and rotates. A particularly useful result is an error checking algorithm that graphically displays the regions where most errors occur. The SAR interpretation algorithms developed under this research funding have contributed to the Geophysical Data Processing System (GPS) at the Alaskan SAR Facility (ASF) in Fairbanks, Alaska. The geophysical data flowing from this system are in use in the Joint Ice Center (JIC) as well as the Naval Polar Oceanography Center (NPOC) and the remote sensing activities of the Naval Research Laboratory, Detachment South. The SAR interpretation algorithms to which this research contributes assure that SAR image information is available in a timely manner for use in ice science and naval applications.

TABLE of CONTENTS

I. Introduction and Motivation for Sea Ice Research

Sea ice is of fundamental importance in weather, climate and other geophysical processes. It is also an important factor for naval operations in the polar regions, in particular regarding transport of personnel and material in regions where sea ice is likely to be found and assessment and prediction of acoustic environments in polar regions. Because sea ice has a large geographic extent and short time scale for variability synthetic aperture radar (SAR) is a valuable technique in studying sea ice. A SAR image is a 'radar picture' of a scene on the Earth's surface. The picture elements or pixels of the scene are a map of the radar reflectivity of the pixel's area on the surface. SAR images are particularly useful in that they can be collected through clouds and at night. Such a capability is clearly important in polar regions. SAR information on sea ice will be available from several satellites in the 1990's (ERS-1, JERS-1, Almaz, Radarsat and possibly an EOS SAR). Automated interpretation techniques are required because of the large number and high information content of the SAR images becoming available. We have worked to develop automated-computer-based techniques for such interpretation and make use of advanced methods and concepts in image processing, computer vision and artificial intelligence.

The general problem that we face is to extract geophysical information from one or more SAR images. The work reported here concerns estimation of sea ice motion. Hence, we collect two images of a given geographical area some several days apart and note the change in sea ice location which gives us the average sea ice velocity vector. While one can do this manually by establishing tie points on the same piece of ice in the two scenes, an automated algorithm is preferable for both cost and consistency reasons. The research reported here contains important results for the solution of this problem.

The SAR interpretation algorithms developed under this research funding have have contributed to the Geophysical Data Processing System (GPS) at the Alaskan SAR Facility (ASF) in Fairbanks, Alaska. The geophysical data flowing from this system are in use in the Joint Ice Center (JIC) as well as the Naval Polar Oceanography Center (NPOC) and the remote sensing activities of the Naval Research Laboratory, Detachment South. The SAR interpretation algorithms to which this research contributes assure that SAR image information is available in a timely manner for use in ice science and naval applications.

An example of the contribution that our results have made is illustrated in Fig. 6 on p. 63 of Vesecky et al. (1988) -- see the Appendix, beginning on page 12, for a copy of this paper. Our general scheme for ice tracking, illustrated in Fig. 6, was first presented in 1988 and eventually lead to the basis for the algorithm implemented in the Geophysical Processor at the ASF. Ideas in the results reported here were fundamental to both the general scheme of the ice tracking algorithm as well as the components within the algorithm.

II. Research Objectives

The objectives of research reported here follow from the circumstances discussed above. The objectives can be summarized as follows:

1. Investigate methods for estimating sea ice motion given two more SAR images of sea ice fields, collected at intervals of the order of days.

2. Develop the methods above into working computational algorithms that function in an automated fashion.

3. Test the algorithms above on image pairs collected by Seasat SAR and a variety of aircraft SAR images.

5. Modify the algorithms of item 2 in the light of 3 until satisfactory performance is achieved.

6. Support the implementation of the algorithms developed on the Geophysical Processor System of the Alaskan SAR Facility.

III. Research Results

The research results stemming from the objectives above can be summarized under four topics:

A. Image pyramid area correlation schemes
B. Feature tracing schemes
C. Rotation invariant correlation
D. Checking results by image subtraction.

The most significant progress made on these topics concerns the first two. The results in these two areas are incorporated in the sea ice tracking algorithms now in place at the Alaskan SAR Facility at the University of Alaska in Fairbanks.

A. Image Pyramid Area Correlation Schemes

For tracking of sea ice that translates without significant rotation the image pyramid area correlation scheme has proved to be a robust method of ice tracking. In this scheme a sequence of images or image pyramid is constructed in which each image in the sequence has progressively cruder resolution. A typical scheme is to average 4 pixels in one scene to produce the next image in the sequence. The pyramid refers to the fact that as resolution is degraded the images have fewer pixels (covering more surface area each) and the images become smaller in terms of pixels although the image corresponds to the same geographical area. These progressively smaller images can be stacked up to form a pyramid as shown in Fig. 1 of Vesecky et al. (1988a) in the Appendix.

The image pyramid area correlation method for ice tracking begins with the crude resolution image pair at the top of the pyramid. A small square block of pixels, a subimage, in the first image, image 1, of a pair is selected and cross correlated with areas in the second image of the pair, image 2. The region with highest correlation in image 2 shows where the ice in the selected subimage has moved over the several days between the collection of image 1 and image 2. This process is repeated for all the non-overlapping subimages of image 1. The result is a field of vectors showing a crude estimate of the large scale ice motion field. The process is repeated with the next image pair in the pyramid, i.e. with slightly better resolution. However, we now have a general idea of the large scale motion field; so we know approximately where to conduct our correlation search -- we don't have to cross correlate with all of image 2, just a suitable, small part of it. After the process has been repeated several times we arrive at the base of the image pyramid, obtaining the highest resolution velocity vector field. At each step we have used the velocity field estimate at the next higher level to guide our search for the highest cross correlation match. Results of this algorithm are shown in Fig. 2 of Vesecky et al. (1988a) or Fig. 4. of Vesecky et al. (1988b).

B. Feature Tracking Schemes

While the image pyramid area correlation method works very robustly on ice that translates, but does not rotate, it begins to break down when the ice in the image rotates or shears. As shown in Vesecky et al. (1988a), a rotation of only 7° reduces correlation in a typical SAR sea ice image to 0.8. A shear of about 10° is required to reduce the correlation to 0.8. Thus, even a small amount of rotation or shear can cause mistakes in the image pyramid method. Regions where such errors are likely to occur can be recognized by the fact that the maximum cross correlation is reduced below 0.8. In such regions it is necessary to use another method or to expand the IPAC scheme to account for rotation. Expanding the IPAC to include all possible rotations would mean expanding the search space by a factor of 50 or more with the associated increase in computation load. Hence, a second method appears attractive.

Feature tracking seeks to decompose each SAR sea ice image into a collection of features. Vesecky et al. (1988b) did this for the first time. The features used were segments of the edges of floes as shown in Fig. 9 of the above reference (reproduced in the Appendix). The trick here is that the features are characterized independent of their orientation. One then seeks to find a matching pair of features in both images. Once a matching pair of features is found both the translation and rotation of the ice are known. While the feature tracking scheme does not yield a complete ice velocity map, it does show portions of the map indicating where rotation occurs. Thus, by using feature tracking one can determine the amount of translation and rotation in a particular region and adapt IPAC by knowing the amount of rotation to apply when searching for corresponding regions in an image pair.

A useful approach to tracking sea ice that rotates is to use a combination of IPAC and feature tracking, as suggested in Vesecky et al. (1988a). For example, one could first run the feature tracking algorithm, noting regions of significant rotation. This information would be used as part of the guided search for matching regions in IPAC. An alternative would be to run IPAC first and then seek feature tracking information only in those regions where no high correlation matches were found. In these 'no match' cases feature tracking would be done to provide rotation information so that a match could be found. Schemes such as these are now used in the geophysical processor at the Alaskan SAR Facility (ASF) in Fairbanks.

C. Rotation Invarient Correlation

Another approach to tracking ice that rotates is rotation invariant correlation. Vesecky et al. (1987) applied the rotation invariant moments of Hu (1972) to the tracking of rotating sea ice floes. Although the method worked reasonably well on the floes tested, it did not seem as likely to succeed as the feature tracking. Hence, it was not pursued.

D. Checking Results by Image Subtraction

A very useful technique was developed to check the results of ice tracking algorithms. The idea is first to estimate the velocity field from a given image pair. Then, using this velocity field, transport the pixels in the first image to a new position and form an estimate of the second image in the pair. This second image estimate is then subtracted from the observed second image and a difference image constructed. One can then easily see where the velocity field estimate is in error. Often the regions where there are groups of errors are regions of significant ice shear and distortion because the ice is so broken up that there are no coherent pieces as large as ten or twenty pixels. An example of this type of check is given in Vesecky et al. (1988b).

IV. Applications of Results

The results of the work performed here have been primarily used in the algorithms in place in the ice tracking portion of the Geophysical Processing System (GPS) at the Alaskan SAR Facility, Geophysical Institute, University of Alaska, Fairbanks. In particular we were the first to develop automated feature tracking and the first to formulate the basics of the processor strategy that uses both feature tracking and image pyramid area correlation (IPAC) techniques. The data products from the GPS go to Navy users via the Joint Ice Center (JIC). The primary data products from the GPS are ice classification maps from ERS-1 SAR images and ice motion maps from pairs of ERS-1 SAR images. Data from the Japanese JERS-1 SAR are also now becoming available.

The results of our work have also been communicated to research workers in the European community for use in analysis and interpretation or ERS-1 SAR images collected at Canadian, British, Norwegian, German and Swedish ground stations.

V. Conclusions

The primary conclusions of this research can be summarized as follows:

1. Automated processing schemes are capable of estimating sea ice movement from pairs of SAR images under a wide variety of conditions.

2. The image pyramid area correlation algorithm when combined with feature tracking methods can form a robust ice velocity algorithm.

3. The tracking of rotating ice can be handled by either feature tracking or rotation invariant correlation.

4. An excellent scheme for checking ice velocity estimates is to use them to estimate the second image of a pair by transporting the pixels from the first image. The estimate of the second image is then subtracted from the observed second image and regions of error are strikingly displayed.

REFERENCES

Hu, M-K, Visual pattern recognition by moment invariants, **IRE Trans. Infor. Th., 8**, 179-187 (1962).

Jain, A. K., **Fundamentals of Image Processing**, Prentice-Hall, Englewood Cliffs NJ (1989).

VI. BIBLIOGRAPHY

Ph. D. Thesis:

Ramin Samadani: "Image Pyramid Motion Detection Applied to Sea Ice" Ph. D., Electrical Engineering, Stanford University (1987).

Journal Paper:

Vesecky, J. F., R. Samadani, M. P. Smith, J. M. Daida, and R. N. Bracewell, "Observation of sea ice dynamics using synthetic aperture radar: automated analysis", **IEEE Trans. Geosci. & Rem. Sensing, 26**, 1, 38-48 (Jan., 1988b).

Conference and Symposia Papers:

Vesecky, J. F., R. Samadani, M. P. Smith, J. M. Daida and R. N. Bracewell, "Automated Remote Sensing of Sea Ice Using Synthetic Aperture Radar", **Proceeding of IGARSS '86 Symp.**, ESA Document SP-254, 127-132, European Space Agency, Paris (1986) --Invited Paper.

Vesecky, J. F., R. Samadani, J. M. Daida, M. P. Smith and R. N. Bracewell, "Observing Rotation and Deformation of Sea Ice with Synthetic Aperture Radar", **Proc. IGARSS 87 Conf.**, 1137-1146, IEEE Press, Piscataway NJ (May, 1987).

Vesecky, J. F., R. Samadani, J. M. Daida, M. P. Smith and R. N. Bracewell, "Observation of sea ice motion and deformation using synthetic aperture radar: automated analysis algorithms", **Instrumentation and Measurements in the Polar Regions** (W. W. Denner, ed.), 47-66, Marine Technology Society, Berkeley CA (Jan.,1988a).

Vesecky, J. F., R. Samadani, J. M. Daida, M. P. Smith and R. N. Bracewell, "Remote sensing of sea ice motion using floe edge and pressure ridge features in SAR images", 417-418, **IGARSS' 88 Conf. Proc.**, ESA SP-284, European Space Agency, Paris (Sept, 1988c).

APPENDIX of PAPERS

PUBLISHED under ONR SPONSORSHIP

1986-1988

Observation of Sea-Ice Dynamics Using Synthetic Aperture Radar Images: Automated Analysis

John F. Vesecky
Ramin Samadani
Martha P. Smith
Jason M. Daida
Ronald N. Bracewell

Reprinted from
IEEE TRANSACTIONS ON GEOSCIENCE AND REMOTE SENSING
Vol. GE-26, No. 1, January 1988

Observation of Sea-Ice Dynamics Using Synthetic Aperture Radar Images: Automated Analysis

JOHN F. VESECKY, MEMBER, IEEE, RAMIN SAMADANI, MARTHA P. SMITH, JASON M. DAIDA, AND RONALD N. BRACEWELL, FELLOW, IEEE

Abstract—Synthetic aperture radar (SAR) provides an excellent means of observing the movement and distortion of sea ice over large temporal and spatial scales. SAR observations are not affected by clouds or lack of sunlight. The European Space Agency's ERS-1 satellite as well as others planned to follow will carry SAR's over the polar regions beginning in 1989. A key component in utilization of these SAR data is an automated scheme for extracting the sea-ice velocity field from a time sequence of SAR images of the same geographical region. We briefly describe two techniques for automated sea-ice tracking: image pyramid area correlation (hierarchical correlation) and feature tracking. Each of these techniques is applied to a pair of Seasat SAR sea-ice images. The results compare well with each other and with manually tracked estimates of the ice velocity field. We note the advantages and disadvantages of each of these automated methods. Using these ice velocity field estimates one can reconstruct one sea-ice image from the other member of the pair. Comparing the reconstructed image with the observed one, errors in the estimated velocity field can be recognized and a useful probable error display created automatically to accompany ice velocity estimates. We also suggest that this error display may be useful in segmenting the sea ice observed into regions that move as rigid plates and regions of significant ice velocity shear and distortion.

I. INTRODUCTION

THE IMPORTANCE of sea-ice remote sensing arises from the high spatial and temporal variability of sea ice, its wide geographic extent, and its impact on climate, arctic offshore engineering, transportation, and military operations. Sea ice dramatically changes the air-sea energy balance and energy transport. Since sea ice can cover significant areas of the Arctic and Southern Oceans, it has an important impact on both polar and global climate.

The high variability of sea ice coupled with its large extent makes remote-sensing techniques a necessity for large-scale studies. Since polar regions are often cloud covered and without sunlight for long periods, the ability of synthetic aperture radar (SAR) to provide areally extensive high-resolution images through clouds and without sunlight gives it a central role in sea-ice remote sensing. SAR provides good information on sea-ice extent, movement and deformation, internal geometry (structure of floes and leads), and surface roughness [1]. Some useful information on sea-ice types and their physical properties can also be obtained from SAR images.

The process of retrieving motion information from a sequence of SAR images (of the same geographic area) revolves around two principal items, namely:

1) Identifying regions in a sea-ice field to use as "tie points" for ice floe tracking.
2) Finding the same tie points in subsequent images of the sequence.

Once the ice displacement is known the ice velocity can be calculated easily since the elapsed time between the SAR images is known. In this paper we shall consider the ice velocity and displacement fields as equivalent since they are simply related by a scale factor.

This process has been carried out manually on Seasat SAR data by Thorndike and Rothrock [1] using a split-screen video display and an experienced operator. Ice velocity is computed automatically once the locations of tie points are marked in a pair of images on the screen. Further work on satellite imagery using manual techniques has been done by Carsey *et al.* [2] and by Curlander, Holt, and Hussey [3]. However, this process is too slow and expensive for real time and/or extensive analysis of images provided by long-term satellite SAR's. Two and possibly three such satellite SAR's are scheduled to be in orbit by the 1990's, namely the European Space Agency ERS-1, the Japanese ERS-1, and the joint Canadian-US-UK Radarsat. Real aperture radar images at low resolution are apparently available from the Soviet Kosmos 1500 series satellites. Hence, the development of automated techniques for floe tracking is a primary requirement for successful use of satellite SAR images in sea-ice remote sensing.

This paper compares two approaches that offer good prospects for automatically retrieving sea-ice velocity information from SAR images and presents a method for assessing the errors in the derived ice velocity field. The two techniques compared here are called "image pyramid area correlation" (IPAC), discussed in Section II, and "boundary segment feature tracking" (BSFT), discussed in Section III. The first technique, also known as "hierarchical correlation," comes from the field of pattern recognition and was first applied to the tracking of sea ice by Fily and Rothrock [4]. Cross-correlation of small blocks

Manuscript received January 29, 1987; revised August 3, 1987. This work was supported by NASA Oceanic Processes, the Office of Naval Research, Code 1125RS, and the Center for Aeronautics and Space Information Systems, Stanford, EECS, NASA Grant NAGW 419.

The authors are with the Space, Telecommunications, and Radioscience Laboratory, Electrical Engineering Department, Stanford University, Stanford, CA 94305-4055.

IEEE Log Number 8717529.

of pixels from a pair of cospatial images is used to find matching scene points. This is made computationally efficient by first building from each primary high-resolution image a sequence (pyramid) of derived images of progressively coarser resolution, but correspondingly fewer data points. Block cross correlation in the coarsest resolution images of the pyramid is computationally fast and builds a crude model of the displacement field of the sea ice. This crude model is then used to guide searches in the pyramid of progressively higher resolution images. As one moves down the pyramid to the highest resolution image, searches are guided from previous results and the displacement field is continually refined. In this paper we discuss methods of rejecting low-confidence ice displacement estimates and interpolating to fill in the rejected data. We also present ice motion characteristics, divergence, and curl, derived from the velocity field.

The second technique, discussed in Section III, also comes from the field of pattern recognition. Our application to the ice tracing problem is new. This method corresponds more closely to the manual (visual) technique than does the image pyramid scheme. Distinctive features are located in the reference (initial) image and then located again in the test (subsequent) image. For our features we use segments of floe-lead boundaries. Thus, each image becomes a set of boundary segment features. The set of features in the reference image forms the tie points, which are then located in the test image and used to derive the ice displacement (velocity) field. We report the results of applying this technique to Seasat SAR images of sea ice.

In Section IV we compare the techniques of Sections II and III, citing the advantages and disadvantages of each. Section V contains new results applying image reconstruction and image subtraction to SAR sea-ice image pairs. These methods are used to identify regions where ice displacement estimates are in error. We also note that the regions of high error density correspond to regions of shear and deformation in the sea ice. This paper ends with Section VI, a summary of conclusions drawn from the results reported.

II. Image Pyramid Area Correlation (IPAC) Method

A. Description of Method

The problem of tracing sea ice from two radar images can be solved by finding a correspondence between the two images at points that represent the same scene point. Examples of *SAR* images of sea ice are given in Fig. 1, where the upper image is from Seasat orbit 1439 (Oct. 5, 1978) and the lower is from orbit 1482 (Oct. 8, 1978), and by Weller *et al.* [1]. Cross-correlation of blocks of pixels in the images can be used to find matching scene points in the images. The displacement vector between matching points is taken to be between centroids of the blocks with the largest correlation coefficient. This displacement information, together with the times of acquisition of the images, can be used to derive velocity information. However, correlation is one of the most computationally expensive image-processing algorithms. One way to speed up the computation is to apply the correlation to an image pyramid data structure. This was first done for sea ice by Fily and Rothrock [4].

An image pyramid, shown in Fig. 1, can be viewed as a set of images in a stack. At the bottom of the stack is the original image and at each of the following levels of the stack is a lower resolution image derived from the level below it by first applying a low pass filter and then resampling the image. The result is a pyramid in which as one traverses from bottom to top, the number of pixels in the images decreases geometrically.

The following steps are needed for effective correlation in a pyramid structure. To begin, pyramids (1 and 2) are constructed (see Fig. 1); one for each of the two images. Then the following algorithm is used:

1) For each I × I pixel sample block in the coarsest level of pyramid 1, calculate a displacement vector by finding the global maximum of the correlation with the coarsest level of pyramid 2. Generate a confidence measure for the displacements.

2) For each finer resolution level of the pyramid do the following:

a) Smooth the displacement vector field for the previous (coarser) pyramid level in order to remove gross errors. This helps prevent errors in the top levels of the pyramid propagating to the lower levels.
b) Interpolate the displacement vector field calculated at the previous pyramid level to provide displacement estimates for each I × I pixel sample block of the current level of pyramid 1.
c) For each I × I pixel sample block of the current level of pyramid 1 find the local maximum of the correlation with the current level of pyramid 2 by searching in an M × M window centered at the displacement estimate of the current level of pyramid 2.

The algorithm starts at the top, coarsest pyramid level and proceeds "top-down" one level at a time. At the coarsest level, the area to be searched in the second image is not constrained, i.e., M is the dimension of the entire image. At each successive level in the pyramid, the estimated location of the largest correlation found at the previous, coarser pyramid level constrains the locations searched. These location constraints greatly decrease the total number of locations that must be searched. The overall gain in speed over brute-force correlation is between 100 and 1000.

The selection of the size (I) of the correlation sample block involves a trade-off between accurate determination of the location of correlation maximum (small I) and avoidance of false correlation maxima (large I). Vesecky *et al.* [5] describe a cross-correlation technique for choosing I. The choice of I is dependent on image content. For the sea-ice image of Fig. 1, an I corresponding to about

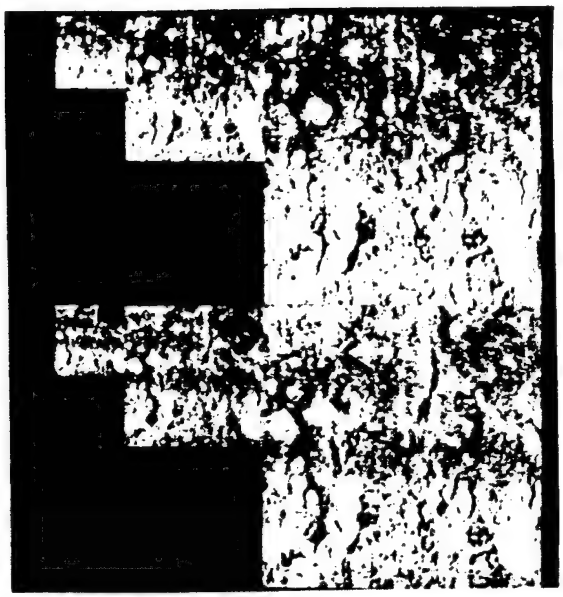

Fig. 1. Image pyramids for two Seasat SAR images of the same central pack ice area in the Beaufort Sea. The images were collected three days apart on Oct. 5 and 8, 1978 on orbits 1439 and 1482.

a 4 × 4 km block size was judged to be near optimum, i.e., I = 16 for 250-m size pixels. This size is of the order of the size of the average ice floe.

The quantity M is selected to correspond to a search area of the order of the physical size of the correlation sample block in the coarser pyramid level just processed. We have taken M such that the search area is four times larger then the previous (coarser) level sample block size.

B. First-Order Results for Seasat SAR Image Pair

We applied the pyramid algorithm described above to two averaged (250-m pixels) Seasat images of central arctic pack sea ice–Rev. 1439 (October 5, 1978) and Rev. 1482 (October 8, 1978) [6]. The experiment used three-level pyramids. A median filter was used for the smoothing of the displacement vectors. Bilinear interpolation was used for the interpolation of the displacement vectors. Fig. 2(a) shows the displacement vectors at the finest resolution. The direction of most vectors is from top to bottom. Comparing these displacement vectors with a computer-assisted manual analysis by Thorndike and Rothrock [1] shown in Fig. 2(b), it is seen that the method performs very well. However, there are areas where the automated algorithm has generated erroneous velocity vectors. The problem areas at the edges of the figure correspond to ice features flowing into or out of the finite area of these images.

C. Confidence Estimates

There are two parts of the pyramid algorithm where confidence measures are useful. For the final vector output, confidence measures can be used to prune or to at least highlight suspect vectors. In addition, during the interpolations from a coarser pyramid level to a finer pyramid level, the confidence measures can be used as a weighting factor for the interpolation [7]. The first technique was used in obtaining the results reported here.

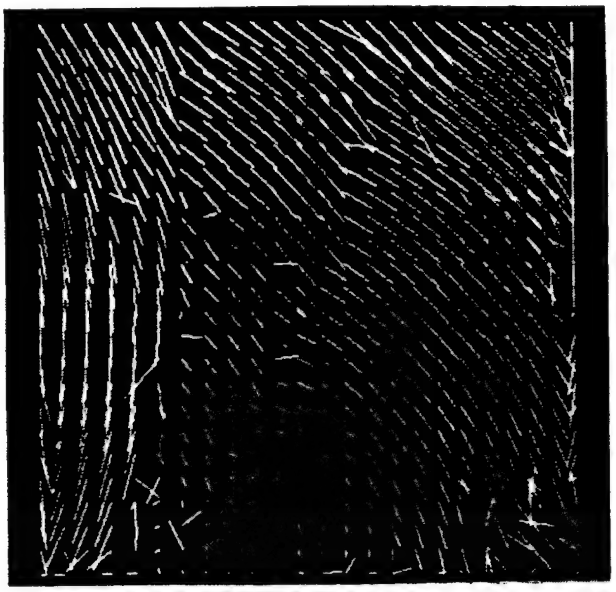

(a)

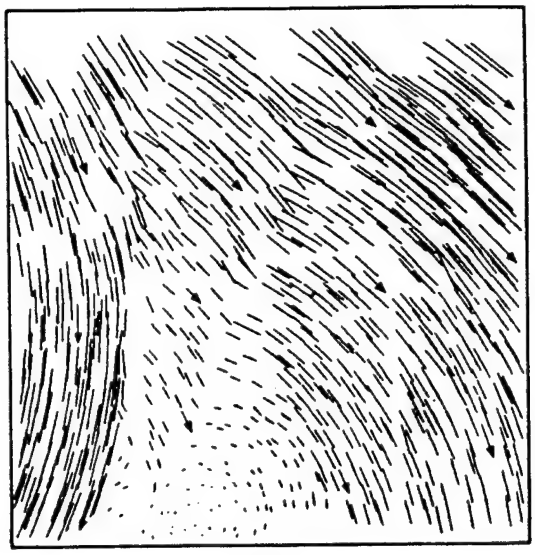

(b)

Fig. 2. (a) Sea-ice velocity vectors generated by the image pyramid area correlation technique (IPAC) applied to the SAR images of Fig. 1. (b) Sea-ice velocity vectors generated from the same image data of Fig. 1 by Thorndike and Rothrock [1] using a computer-assisted manual technique. The velocity estimates of (a) are improved by pruning of low confidence estimates and replacement by interpolation as shown in Fig. 4.

The coordinates of the maximum correlation for a block provide the value for its velocity vector. The values of the correlation surface near the maximum may provide a confidence measure to be associated with the velocity vectors. Fig. 3 shows the value of the correlation coefficient superimposed on the velocity vectors. The correlation coefficient is being used as a measure of confidence, with brighter regions signifying high confidence and darker regions signifying low confidence. It is seen that there is a correspondence between areas of low confidence and errors in the displacement field.

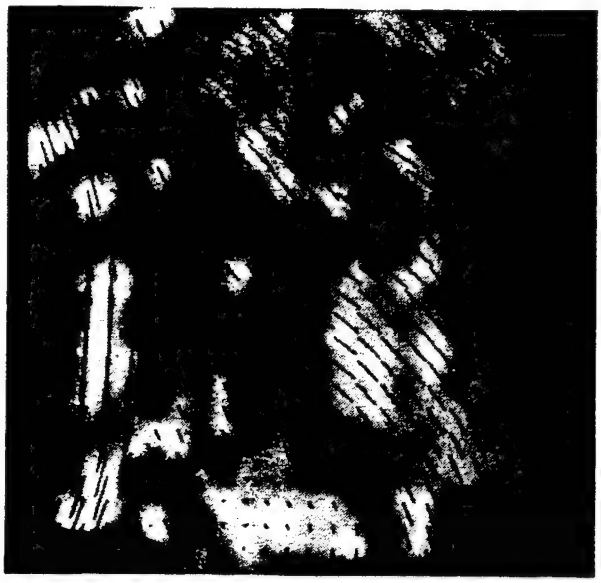

Fig. 3. Confidence estimates for sea-ice velocity vectors generated by the automated image pyramid area correlation technique (IPAC). The bright shades denote regions of high confidence and the dark areas, regions of low confidence. The ice velocity field is superimposed on the confidence estimates, which are based on the magnitude of the cross-correlation coefficient for that particular velocity estimate.

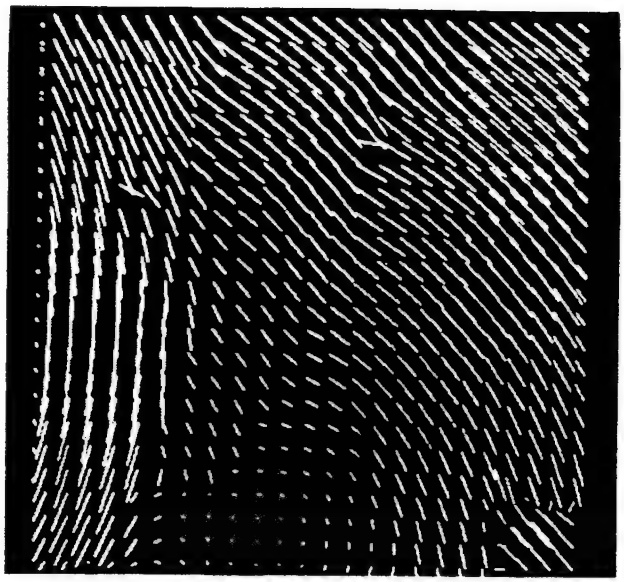

Fig. 4. Ice velocity field of Fig. 2(a) after pruning the low confidence vectors and using the controlled-continuity spline technique for interpolation.

D. Smoothing Techniques

In the "real" world of sea-ice remote sensing using SAR images one encounters noise, grey level variation across a given image and between images, and gross geometric distortions. These problems result in errors when block correlation is used for finding ice displacement vectors. In view of these problems, the assumption is usually made that the displacement field is smooth for most areas of the image [8]. Smoothing techniques may be used to remove the gross errors in the displacement field. These techniques are especially important for pyramid correlation because errors made at the coarser resolutions propagate to the finer levels due to the constraints on search locations at the finer levels. One must be careful when using smoothing techniques, however, in areas where there is high shear.

In the algorithm described in Section II-A smoothing of the estimated ice velocity field was done at each pyramid level by the following procedure. The coarse level vectors were replaced by the median of the surrounding high confidence vectors. Bilinear interpolation was then used to fill in vectors for the next higher resolution level in the pyramid. At the highest resolution level of the pyramid this procedure produced the result of Fig. 2(a).

To improve the result of Fig. 2(a) we have implemented a different smoothing technique by extending the controlled-continuity splines method of Terzopoulos [9] for fitting vector fields. This more versatile interpolation technique makes systematic use of the confidence measure and minimizes the weighted square deviation from the displacement data while at the same time minimizing the integral of the second spatial derivatives. The solution to the minimization problem is via finite elements. The resulting matrix equation is solved via a multigrid relaxation technique using the Gauss-Seidel method for intralevel computations.

Fig. 4 shows the velocity field after pruning the low confidence vectors and using controlled-continuity splines for interpolation. This surface fitting technique could be extended to allow discontinuities in the smoothing process and thus provide a viable smoothing method for areas with velocity shear.

E. Divergence and Curl

We have evaluated the divergence and curl of the computed displacement field, which may be considered to be an averaged velocity field. The displacement field was first smoothed as in Fig. 4; numerical derivatives were then computed. This smoothing reduces the effect of finite block size on estimates of spatial derivatives. Fig. 5(a) shows the divergence of the velocity field. Sinks are shown as dark areas in the image and sources are shown as bright areas in the image. Within rigid blocks, the intermediate gray level signifies zero divergence, as expected. At block boundaries, however, the relative motions of the blocks result in nonzero divergence. Comparing the divergence plot of 5(a) with the sea-ice images of Fig. 1 we note that the bright source region in the lower left quadrant corresponds to a region where the open water area increases between the 5 (upper) and 8 (lower) October images. A similar source feature occurs at the upper center of 5(a). Fig. 5(b) shows the curl of the field. Since the curl of a two-dimensional field has only one component, it can be represented as a scalar. The curl at the center of a clockwise rotation is shown as a brighter area. The curl at the center of a counterclockwise rotation is shown as a darker area.

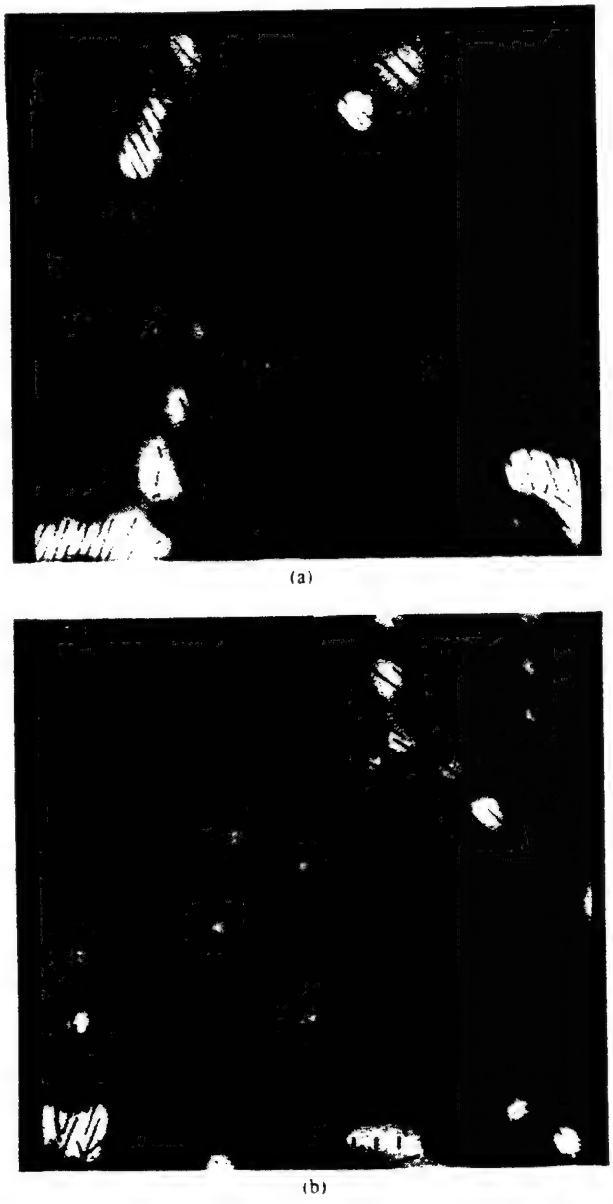

(a)

(b)

Fig. 5. Divergence (a) and curl (b) of the smoothed ice velocity field of Fig. 4. In (a) sinks are shown as dark areas in the image and sources as bright areas. Gray areas signify zero divergence. Since the curl of a two-dimensional field has only one component, it can be represented as a scalar. The curl at the center of a clockwise rotation is shown as a brighter area. The curl at the center of a counterclockwise rotation is shown as a darker area.

III. Feature Tracking With Floe-Lead Boundaries

A. Introduction to the Method

The second algorithm approaches the problem of sea-ice tracking somewhat differently by relying on selected sea-ice features rather than on the content of the entire image. There are a wide variety of features in sea ice that one could track, including pressure ridges, isolated floes, and floe-lead boundaries. Here we have chosen floe-lead boundaries as the physical feature we will track because they are usually the most prominent, distinct, and high constrast features in SAR images of sea ice. The movement of these features from one image to the next provides the information from which the sea-ice velocity field is estimated. Feature patterns must be very distinctive, if not unique, objects. They are characterized by information that is independent of the object location and orientation, though this latter information is, of course, attached to them.

In the feature tracking method each image is transformed into a set of features described by parameters independent of the feature location and orientation. The collection of several hundred features, each described by several hundred numbers, reduces the information needed to characterize a 100 × 100 km image by roughly two orders of magnitude. The search space is correspondingly reduced.

Once a feature pattern is recognized in both members of a pair of images, sea-ice displacement and, hence, velocity information, can be derived. Since we know the movement of every pixel in the feature, we can derive not just one, but many velocity vectors. Further, we know the rotation as well as the displacement of a feature, since we keep track of a feature's geographic orientation in both images of the pair. The results shown here are for floe-lead boundaries; however, the method can also be applied to other features such as pressure ridges or isolated floes.

B. Description of the Feature Tracking Algorithm

The feature tracking algorithm can best be understood by first considering the overview in Fig. 6 and then discussing each component in turn. Following Fig. 6, each image is first averaged to a resolution of about 250 m. Ice and lead are then classified by a simple intensity threshold and floe-lead boundaries are identified. Pixels along floe-lead boundaries are classified and assembled into segments. These boundary segments are characterized and thus form the features that are tracked from one SAR image to another collected three days later. Several tracking passes are made through the collections of features in each image. The high confidence ice displacement estimates, corresponding to high correlation between the characteristics of matching features in the two images, are used to guide the search for other matching features and thus more ice displacement estimates.

Referring to the algorithm block diagram of Fig. 6, we first average both SAR images of a pair to increase the pixel size from the original 25 × 25 m size to 250 × 250 m size. Averaging reduces the speckle variance inherent in SAR images and make computation more tractable since there are a factor of 100 fewer pixels to deal with after averaging. Since SAR pixels cannot be located geographically to better than about 200 m, the average process results in little loss of velocity measurement accuracy.

Proceeding down the block diagram of Fig. 6, a histogram of pixel intensity is formed and a simple pixel intensity threshold is chosen to distinguish between ice floes and leads. Fily and Rothrock [4] have shown that this technique is viable for an example SAR image of central pack ice. Thus, the SAR image pair can be transformed into a pair of images with binary pixels, i.e., 1 for ice floe pixels and 0 for lead water pixels (including new ice). In

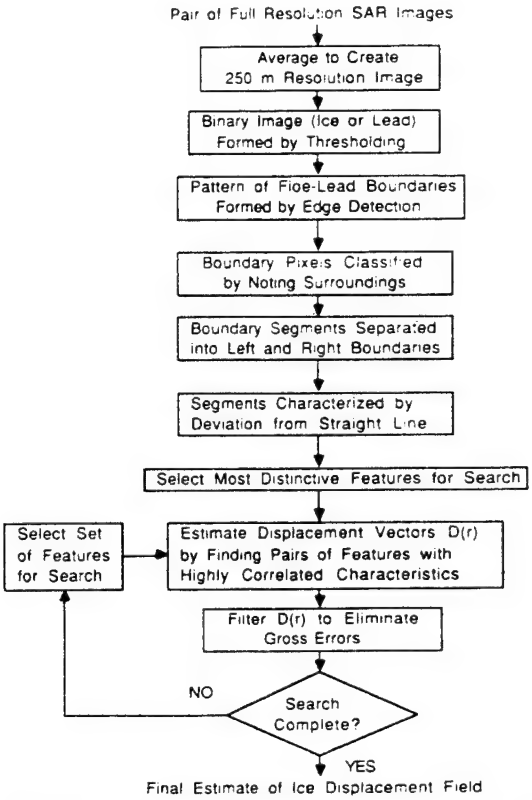

Fig. 6. Block diagram of feature tracking method using floe-lead boundaries.

the next block of Fig. 6 we identify floe-lead boundary pixels simply by finding water pixels adjacent to ice pixels.

In the next block of Fig. 6 the ice-water boundary pixels identified above are classified into eight types according to their surroundings to determine the orientation of the floe-lead boundary edge. The four nearest neighbor pixels are considered to find if there is water above, below, or to the right or to the left of a given boundary pixel. This scheme is illustrated in Fig. 7.

The classified pixels are then assembled into boundary segments that are the features to be tracked. The assembly scheme used here begins by finding the dominant boundary direction. This is done by finding the dominant edge pixel types of Fig. 7. For example, if types 3 and 7 are most common the dominant boundary direction is vertical in Fig. 7. In this example we would then divide our boundary segments into two groups, corresponding to the left and right edges of the leads in Fig. 1, to wit:

Left Edges: edge pixel types 2, 3, 4 and associated types 1 and 5
Right edges: edge pixel types 6, 7, 8 and associated types 1 and 5.

Our aim then would be to match left edges in one image with left edges in the other image and, independently, right edges in the two images. This allows the ice floes along the left side of a lead to slip with respect to ice floes along the right side. Thus, shear motion, which we would

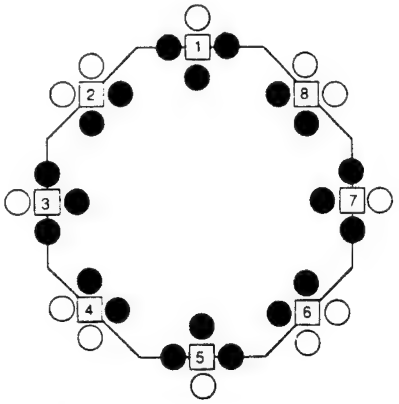

Fig. 7. Diagram illustrating edge pixel classification scheme. The black circles represent water pixels and the white circles ice pixels.

expect across leads in central pack ice, is built into the algorithm for this type of sea ice.

In the next block of Fig. 6 boundary segment features are characterized by their deviation from a straight line. First, a "least squares" criterion straight line is fit to a given boundary segment assembled as above. The distance from this straight line to the segment is calculated at regular intervals along the straight line. This set of deviations characterizes the shape of a boundary segment as illustrated in Fig. 8. Note that this method of characterizing a boundary segment feature is invariant under rotation of the feature.

Recognition of matching features (Fig. 6) is done simply by comparing the sets of deviation measurements for two candidate features. A variance normalized cross-correlation coefficient (C) was used to evaluate how closely two candidate features matched. Often segments that we want to compare are of different lengths because of partial breakup of a boundary segment over the three days between images. So in our search we include features of different lengths. During the comparison process we slide the shorter feature along the longer feature with C calculated for all placements of the smaller feature with respect to the larger. This allows for larger segments to break into smaller ones and still be found.

We have at this point (the entrance to the loop structure in Fig. 6) two images that each contain sets of boundary segments. Because in the central pack ice we do not expect large rotations we have divided each of these sets into left and right edges. The search procedure must select a feature from the reference image (first in time) and try to match it to a feature in the test image (later in time). A successful match reveals ice displacement and, hence, ice velocities at a number of points all along the matching segments.

The search and matching procedure (loop structure in Fig. 6) is an iterative one and has features that remind one of the image pyramid method of Section II above. During the several iterations of the search we use the high confidence ice displacement estimates of the initial iterations to guide the searches of subsequent iterations. In the first iteration only long boundary segments are used since the

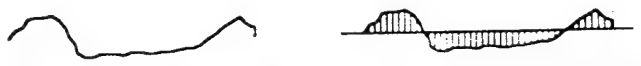

Fig. 8. Boundary segment fitted by a straight line and characterized by deviation from the fitted line.

larger number of pixels gives a more stable estimate of C and a correct match yields ice displacement estimates over a larger region. At this stage for a left boundary segment of n pixels in the reference image we search over left boundary segments with $n/2$ to $2n$ pixels. The search is limited to a displacement of 60–20 km per day for the three days between the images. This search area could be significantly reduced if environmental data such as local winds were available to indicate probable ice movement.

In the first iteration we want to have a very high confidence in our ice displacement estimates. This is because we will use them to guide searches in subsequent iterations. Hence, we require high values of C for a match and reject matches that are not confirmed by nearby matches having roughly similar displacements, $+/-20°$ in direction and $+/-30$ percent in magnitude. In subsequent iterations smaller segments are used, the search region is smaller and guided by previous results, and lower values of C are demanded for a match. In the results reported here seven iterations were made.

C. Application to Seasat SAR Images in the Beaufort Sea

We now apply the boundary segment feature tracking algorithm to the same set of sea-ice images in Fig. 1. We use only the 250 × 250 m pixel size images. Boundary segments constructed from these images vary in length from 4 to 163 pixels or 1 to 41 km in length and have a dominant direction which is vertical, i.e., North-South, in Fig. 1. The resulting sets of boundary segment features in the reference and test images are shown in Fig. 9.

In the initial iteration only the longer segments of image 1439 with lengths greater than 30 pixels (7.5 km) were considered. Thus, in the test image (orbit 1482) matching segments of length $n/2 = 15$ pixels and above were considered in the search. The rather strict criteria on matching features were successful in removing many erroneous matches, although it did also eliminate a few correct matches as well. The subsequent iterations added progressively fewer matches until by the seventh iteration no new matches were found. It has been our experience in developing this algorithm that the primary difficulty lies in making sure incorrect matches are rejected rather than in making sure correct matches are retained.

Fig. 10 shows the resulting ice displacement vectors for the sea-ice image pair of Fig. 1. These displacement vectors agree very well with the manually generated and IPAC displacement vectors of Fig. 2. We note that there are large regions where no displacement vectors are shown. This situation arises from two causes. First, no ice displacement vectors will be generated in regions where there are no lead-floe boundary features to be tracked. The second is that in regions where there is too much deformation, a boundary segment in the reference image will often be too badly broken up in the test image to be recognized. In the first case other features, such as pressure ridge patterns, could be tracked as well as the lead-floe boundary segments. In the second case the use of higher resolution images might be helpful if the deformation were less severe at smaller size scales. A drawback of using higher resolution pixels in SAR images is that speckle noise becomes a significant component of the intensity variation from one pixel to the next.

IV. Comparison of Methods

Given our results, we can qualitatively address some of the advantages and disadvantages that accompany the sea-ice tracking methods considered above. In particular, we can compare the methods using an outline suggested by Kashef and Sawchuck [10].

A feature-matching method, such as the boundary segment feature tracking (BSFT) method of Section III, approaches mat (image) data differently from a correlation method, such as the image pyramid area correlation (IPAC) method of Section II. Whereas correlation methods rely on the intensity values of map data, feature-matching methods rely on detected edges, boundaries, and vertices of map data. The advantage of using BSFT in tracking sea ice lies in reducing an image of millions of pixels to one of, say, thousands of pixels. Only relevant data applies to tracking. The potential cost-savings for computational speed exist, depending on how "relevant" the reduced data are. In particular, one should only pick those edges, boundaries, and vertices common to both images for tracking.

Picking those edges, boundaries, and vertices common to both images remains difficult. Thus, the advantage for BSFT also harbors a disadvantage. Boundaries may fragment or disappear. Furthermore, unrelated boundaries may have similar characteristics and lead to false matches. Finally, some areas of sea ice are virtually featureless, having few discernable floe-lead boundaries.

To address the difficulty in identifying features common to both images, we have adopted a feature tracking algorithm that iterates. For the first pass, feature tracking results in finding five to ten matching features. We use these matches to guide the search for other matches on the next pass. The process repeats. In this way, we have successfully identified a significant number of features common to images for orbit 1439 and orbit 1482. Iterative feature tracking has resulted in a velocity vector map that agrees well with manual tracking results, although the number of velocity vectors located by feature tracking falls short of the number of velocity vectors located either by IPAC or manual tracking. In the case at hand we expect this behavior since only one type of feature was considered.

Correlation methods surmount the difficulty of identifying common features or tie points by allowing a large range of image content: i.e., the algorithms are not dependent on the existence of specific features such as floe-

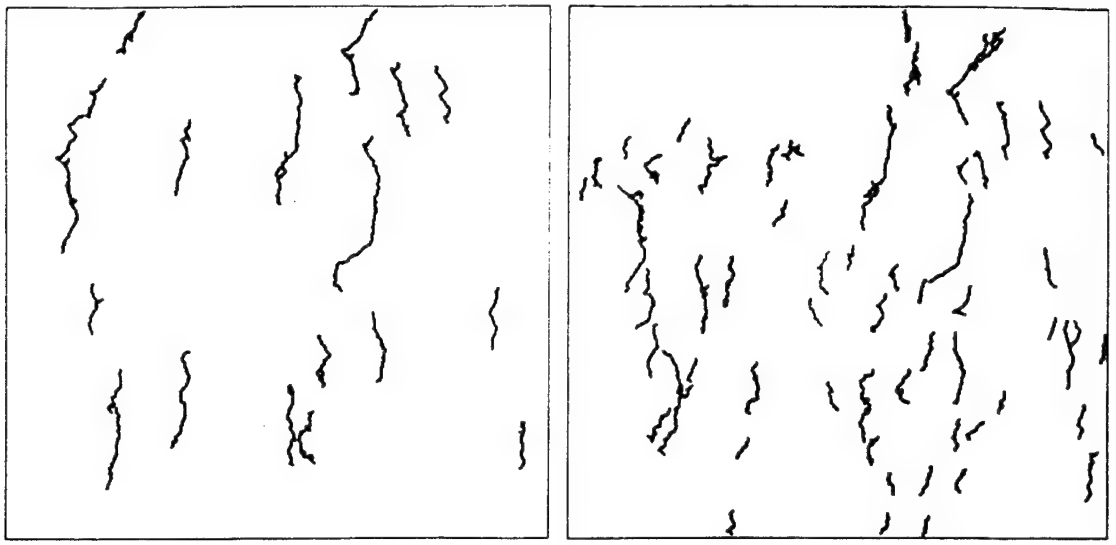

Fig. 9. Search space of long floe-lead boundary segments constructed from orbit 1439 (left) and orbit 1482 (right) SAR image data. Only left edges are shown.

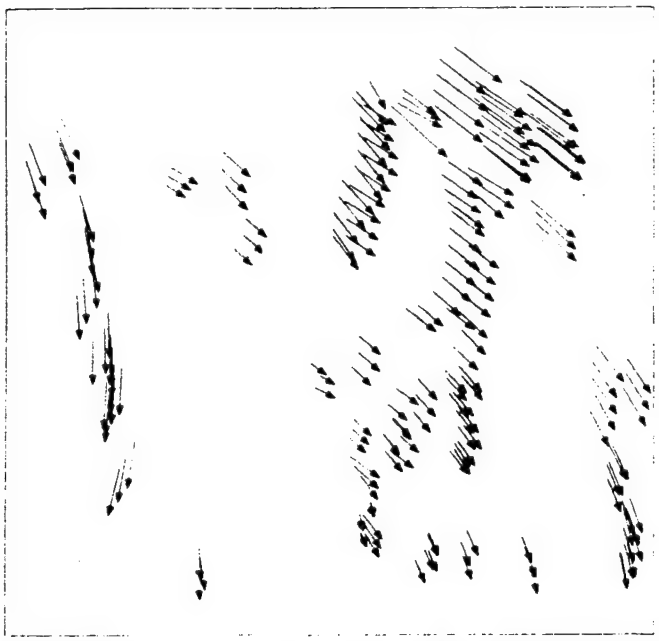

Fig. 10. Ice velocity vectors derived from the SAR images of Fig. 1 using the boundary segment feature tracking (BSFT) algorithm.

lead boundaries. Traditionally, computation-intensive correlation methods become attractive when computation is reduced by the IPAC approach. The noise immunity provided by averaging in IPAC comes as an added bonus. Therefore, the advantage of using IPAC techniques stems threefold: IPAC assumes little about image content; IPAC can track global displacements well; IPAC has inherent noise immunity.

Despite the advantages of IPAC, "image pyramid" techniques, like the one used here, cannot detect small-scale pattern changes that involve a large rotation. This problem is significant given the rotational as well as translational, nature of sea-ice motion. To address this drawback, one can opt for two schemes. One scheme involves substituting at some point a rotation-invariant correlation measure in place of standard correlation. Another approach would be a synthesis from both IPAC and BSFT.

There are other disadvantages to using "image pyramid" techniques. In our research, we have found that IPAC was sensitive to tracking mistakes at the top (course resolution level) of the pyramid. These tracking errors propagated and resulted in some velocity vector estimates significantly different than manual tracking results. For the central pack ice images we have used, we have been able to discard a velocity vector if the correlation coefficient corresponding to it falls below a threshold value and then fill the void by an interpolation scheme. The scheme of discarding velocity vectors judged to be unreliable and interpolating from surrounding vectors to fill in the void can also be applied to BSFT ice velocity estimates. Unfortunately, the same method might not work so well for other sea-ice images; for example, if voids occur over areas too large to interpolate across. Other potential problems using "image pyramid" techniques might arise in areas of nonuniform motion from averaging velocity vector estimates over too many pixels.

Because IPAC and BSFT provide estimates of ice velocity that are independent the two methods are complementary in the sense that agreement between the two methods implies a high confidence estimate of ice velocity. Thus, the two methods could be used together with a single algorithm to provide better sea-ice velocity estimates than either could alone. For example, BSFT velocity estimates could be used to reduce critical IPAC errors in the coarse resolution levels of an image pyramid and to confirm results at finer resolution levels.

V. Error Analysis by Image Reconstruction and Subtraction

A. Image Restoration, Remapping, and Image Subtraction

As stated in the introduction, the goal of this research is to produce ice velocity data for sea-ice science and ap-

plications. To make the ice velocity field estimates of Figs. 2, 4, and 10 truly useful they must be accompanied by some measure of the quality of the estimates. We have found image remapping to be a useful technique for evaluating the quality of a velocity field. The estimated ice velocity field defines a mapping between the pair of images. One can use this mapping to remap the intensities in the second image to the locations they would be found in the first image. When we alternatively display the first image and the remapped second image on the same image display, the areas where the algorithm works well are seen to be static. The areas where the algorithm fails appear to flicker or to move slightly because of errors in the mapping.

With the remapped data available, the absolute difference of the first image and the remapped second image can be produced. In order to understand the significance of the difference technique, the motion detection problem must be expressed as an image restoration problem.

We have modeled the motion process as a linear space-varying transformation of intensities from the first image to the second image. Using this model, the second image may be considered to be a superposition integral involving the impulse response of the motion process and the intensity function of the first image. We further assume that the imaging system does not vary from image to image, and that the correlation algorithm can also be modeled as a space-varying linear process. Then, it can be shown that the difference between the first image and the remapped version of the second image bounds the errors in the motion if there is detail in the image. Intuitively, if the motion algorithm is correct, the remapped intensities subtract perfectly from the original intensities leaving zero remainder. If it is erroneous, then the intensities will not subtract perfectly and the residual errors will be displayed as bright portions in the difference image.

We recognize that in the practical world of SAR remote sensing there are likely to be changes in intensity between the two images in a pair that are unrelated to ice motion. For example, changes in system gain, incidence angle, aspect angle, and surface conditions (such as snow and wind) can cause variations in SAR image intensity. However, the successful results of Fig. 11 resulted from the pair of Seasat SAR images shown in Fig. 1. So we are optimistic that the method will have application to a significant fraction of satellite SAR observations of sea ice, which are less subject to the variations mentioned above than aircraft observations.

B. Error Detection by Image Subtraction

Fig. 11 shows the absolute value of the difference between the Oct. 5 (orbit 1439) image and the remapped Oct. 8 (orbit 1482) image. The remapped Oct. 8 image was created using the smoothed IPAC velocity vector estimates of Fig. 4. The difference picture has been displayed so that image intensity differences greater than a chosen threshold value are bright and those below are dark. Thus, high error regions are bright and low error regions are dark.

Fig. 11. Image reconstruction and subtraction map based on the ice velocity field of Fig. 4. This difference picture is displayed so that absolute image intensity differences greater than a chosen threshold value are bright and those below are dark. Thus, regions where ice velocity estimates are likely to be in error are bright and low error regions are dark.

This image provides a convenient display of the regions where the ice velocity estimates are likely to be in error. Here we have assumed that the ice itself remains the same, as seen by the SAR, in the two images. This error map can be used in two ways. First, it can be used as a guide to the credibility of the ice velocity field estimates provided by SAR. Thus, the ice science or applications user is in a position to know when and where the ice velocity data provided to him are dependable or likely to be in error. Second, the error data can be used as feedback within an ice velocity estimation algorithm to improve the velocity estimates. For example, higher resolution image data, i.e, pixels smaller than the 250 m used here, could be employed to try to resolve errors sensed by the image subtraction technique.

C. Interpretation of Regions Containing Large and Small Errors

By comparing the error display of Fig. 11 with the ice velocity field as shown in Figs. 2, 4, and 10 we find that we can make an interesting interpretation of the error display. First, we note that the large dark areas where errors are low correspond to large blocks of ice that move as rigid plates. These large units were also pointed out by Fily and Rothrock [4]. Second, we see that the large error (bright) regions tend to fall along lines that separate the large rigid plates. It is in these regions that the large plates apparently grind against one another producing velocity shear that deforms the ice. The deformation of the ice in these regions, coupled with the fact that the ice velocity estimates are discrete and smoothed, causes errors in ice velocity estimates.

Thus, we suggest that the remapping error plots such as that shown in Fig. 11 can be used to segment an ice velocity field into dark regions that tend to be large rigidly rotating plates and bright regions where there is much shear and ice deformation. We realize, of course, that this interpretation is based on a single observation. Nevertheless, we think it is worth pointing out since it may well prove to be a useful method of automatically surveying sea-ice velocity fields sensed by SAR or other imaging sensors.

VI. Conclusions

We summarize our conclusions based on the research reported above as follows:

1) For the sea-ice images considered here the image pyramid area correlation (IPAC) algorithm provides a useful, though not ideal, means of automating the process of deriving sea-ice velocity information from SAR images. Rejecting low confidence velocity estimates and replacing them by interpolated values improves IPAC results in comparison with manual results.

2) Feature tracking using floe-lead boundary segments (BSFT) produces a large number of sea-ice velocity estimates that agree well with IPAC and manual results. However, the method cannot comprehensively cover the region observed by the SAR because trackable floe-lead boundaries are not present everywhere. Extension to pressure ridge features is indicated.

3) The IPAC and BSFT algorithms provide independent estimates of sea-ice velocity, both having their advantages and disadvantages. We conclude that the two algorithms complement each other in many ways. An algorithm synthesized from both techniques is indicated.

4) To make remotely sensed ice velocity field data useful in sea-ice science and applications a measure of data quality is needed. We conclude that the image reconstruction and subtraction technique provides such a measure of data quality. The technique may also be useful in segmenting SAR observations of sea ice into rigid plates and regions of significant shear and ice deformation.

Acknowledgment

We are grateful to Dr. F. Carsey, Dr. J. Curlander, and Mr. B. Holt at the NASA Jet Propulsion Laboratory for supplying sea-ice SAR images. S. Barsch and S. Vesecky are acknowledged with thanks for their help in manuscript and figure preparation. The reviewers of this paper provided a mass of useful comments and suggestions that have been incorporated into the paper—we thank them for their thought and time. We gratefully acknowledge guidance and encouragement from NASA Oceanic Processes (Dr. K. Jezek and Dr. R. Thomas) and the Office of Naval Research, Code 1125RS (Mr. C. Luther).

References

[1] G. Weller, F. Carsey, B. Holt, D. A. Rothrock, and W. F. Weeks, "Science program for an imaging radar receiving station in Alaska—Report of the Science Working Group," NASA-Jet Propulsion Lab., Pasadena, CA, 1983.

[2] F. Carsey, J. Curlander, B. Holt, and K. Hussey, "Shear zone ice deformation using supervised analysis on SEASAT data," presented at the A.I.A.A. 21st Aerospace Science Meeting, Reno, Nevada, 1983.

[3] J. Curlander, B. Holt, and K. Hussey, "Determination of sea ice motion using digital SAR imagery," *IEEE J. Ocean. Eng.*, in press, 1987.

[4] M. Fily and D. A. Rothrock, "Extracting sea ice data from satellite SAR imagery," *IEEE Trans. Geosci. Remote Sensing*, vol. GE-24, pp. 849-854, Nov. 1986.

[5] J. F. Vesecky, R. Samadani, M. P. Smith, J. M. Daida, and R. N. Bracewell, "Observing rotation and deformation of sea ice with synthetic aperture radar," in *IGARSS Dig.* (Piscataway, NJ), IEEE Press, pp. 1137-1146, 1987.

[6] ——, "Automated remote sensing of sea ice using synthetic aperture radar," in *IGARSS: Remote Sensing, Today's Solutions for Tomorrow's Information Needs* (Paris), pp. 127-132, ESA Pub. Div., 1986.

[7] P. Anandan and R. Weiss, "Introducting a smoothness constraint in a matching approach for the computation of optical flow fields," in *Proc. IEEE Third Workshop Computer Vision: Representation Control*, pp. 253-257, (Bellaire, MI), Oct. 13-16, 1985.

[8] H. Nagel and W. Enkelmann, "An investigation of smoothness constraints for the estimation of displacement vector fields from image sequences," *IEEE Trans. Pattern Anal. Machine Intell.*, vol. 22, no. 9, pp. 959-967, Sept. 1986.

[9] D. Terzopoulos, "Computing visible-surface representations," MIT Artificial Intelligence Laboratory, A. I. Memo. 800, Mar. 1985.

[10] M. Kashef and A. Sawchuck, "A survey of new techniques for image registration and mapping," in *Applications of Digital Image Processing VI. Proc. SPIE.* (San Diego, CA), 1982.

*

John F. Vesecky (S'61-M'67) received the B.A. and B. S. degrees in electrical engineering from Rice University, Houston, TX, in 1962 and 1963, respectively and the M.S. and Ph.D. degrees from Stanford University, Stanford, CA, in 1965 and 1967.

He was Research Fellow in Astronomy (1967-1969) at Leicester University, U.K. and later taught there in the Astronomy Department (1971-1976) specializing in radio, radar, and X-ray observations of the sun and planets. He did research in radio wave propagation at the Communications and Radio Physics Laboratories at SRI International (1965-1971) and has been with the Electrical Engineering Department of Stanford University in several capacities from 1969-1971 and 1976 to date. He is presently Professor of Electrical Engineering (Research) at Stanford working in radar remote sensing and solar system astronomy. His current research interests include radar remote sensing of sea ice, ice sheets, and ocean winds and waves, acoustic sensing of the marine microlayer, wave scattering from rough surfaces, and spacecraft-earth radar observations of the solar corona and solar wind.

*

Ramin Samadani received the B.S. degree in engineering physics from the University of California, Berkeley, in 1978 and the M.S. degree in electrical engineering from Stanford University, Stanford, CA, in 1981. He is currently working toward the Ph.D. degree at Stanford.

He worked at SRI International in 1978-1979 and at Harris Video Systems in 1981-1982. His fields of interest are image processing and computer vision. His research involves motion detection from images, image pyramid data structures, variational methods applied to image processing, and the scientific applications of image processing.

Martha P. Smith received the A.B. dgree in mathematics from Wilmington College in 1961 and the M.S. degree in chemistry from the University of Wisconsin, Madison, in 1966.

Since 1980 she has been working at the STAR Laboratory at Stanford University where she participates in research involving the analysis of SAR imagery of sea ice and ocean waves.

*

Jason M. Daida received the B.S. degree in electrical engineering from the University of Southern California in 1981 and the M.S. degree in electrical engineering from Stanford University in 1985. He is currently working toward the Ph.D. degree in electrical engineering at Stanford. He holds a Staff Doctoral Fellowship from the Space and Communications Group of Hughes Aircraft Company.

His current research interests include remote sensing, image processing, and active-sensing techniques.

Ronald N. Bracewell (SM'56-F'61) received the B.Sc. degree in mathematics and physics from the University of Sydney, Australia in 1941 and later received the B.E. and M.E. degrees there in 1943 and 1948 with first-class honors. In 1949 he received the Ph.D. degree from the Cavendish Laboratory, Cambridge, U.K.

During World War II he worked on microwave radar at the Commonwealth Scientific and Industrial Research Organization (C.S.I.R.O), Sydney. From 1949 to 1954 he was a Senior Research Officer at C.S.I.R.O., Sydney studying very long wave propagation and radio astronomy. At the University of California, Berkeley, he lectured on radio astronomy in 1954–1955. He also lectured at Stanford University in 1955, joining the faculty of the Electrical Engineering Department in the winter of 1955. He is currently Professor of Electrical Engineering at Stanford. His work at Stanford began in radio astronomy and included the construction and operation of a microwave spectroheliograph and an irregularly spaced radio interferometer for solar and galactic studies. His research work also included satellite motion, computer imaging, solar energy, and extraterrestrial life. He has written a number of books including ones on the Fourier and Hartley transforms. At present he is doing research in computer algorithms for image processing, measurement of ocean surface films and the solar cycle as revealed in Precambrian rocks.

AUTOMATED REMOTE SENSING OF SEA ICE USING SYNTHETIC APERTURE RADAR

J F Vesecky, R Samadani, M P Smith, J M Daida & R N Bracewell

STAR Laboratory, Electrical Engineering Department
Stanford University
Stanford, CA 94305-4055, USA

ABSTRACT

Synthetic aperture radar (SAR) provides an excellent means of observing the movement and distortion of sea ice over large temporal and spatial scales. SAR observations are not affected by clouds or lack of sunlight. The ERS-1 and JERS-1 satellites will carry SAR's over polar regions. A key component in utilization of these SAR data is an automated scheme for extracting the sea ice velocity field from a sequence of SAR images of the same geographical region. We describe two techniques for automated sea ice tracking, image pyramids (hierarchical correlation) and feature tracking. Each of these techniques is applied to a pair of SEASAT SAR sea ice images. The results compare well with each other and manually tracked estimates of the ice velocity field. Finally, we note the advantages and disadvantages of these methods.

1. INTRODUCTION

The importance of sea ice remote sensing arises from the high spatial and temporal variability of sea ice, its wide geographic extent and its impact on climate, arctic off-shore engineering, transportation and military operations. Sea ice dramatically changes the air-sea energy balance and energy transport. Since sea ice covers some 10% of the Arctic and 13% of the Southern Ocean, its impact upon climate is strong.

The high variability of sea ice coupled with its large extent makes remote sensing techniques a necessity for large-scale studies. The ability of synthetic aperture radar to provide large, high resolution images through clouds and without sunlight give it a central role in sea ice remote sensing, especially ice dynamics (Ref. 1). Examples of SAR sea ice images are given in Fig. 1.

The process of retrieving motion information from a sequence of SAR images (of the same geographic area) revolves around two principal items, namely

1. Identification of ice features to use as 'tie points' for ice floe tracking.

2. Finding the same tie points in subsequent images of the sequence.

This process has been accomplished manually using a split-screen video display and an experienced operator. Ice displacement is computed automatically once the locations of a tie point are marked in a pair of images on the screen. Results by Thorndike & Rothrock (in Ref. 1) using this technique are given in Fig. 2 with further work by Carsey et al. and Curlander, Holt and Hussey in Refs. 2&3. However, this process is too slow and expensive for real time and/or extensive use with long-term satellite SAR's such as ERS-1, JERS-1 and RADARSAT. This paper compares two approaches which offer good prospects for automatically retrieving sea ice displacement information from SAR images. The development of an automated technique is a primary requirement for successful use of satellite or aircraft SAR images in sea ice remote sensing.

The two techniques compared here are called the 'image pyramid' and 'boundary segment' sea ice tracking techniques. The most advanced of the two is the image pyramid or hierarchical correlation technique, first applied to sea ice by Fily and Rothrock (Ref. 4). Cross correlation of blocks of pixels from a pair of cospatial images is made computationally efficient by first building from each primary high resolution image a sequence (pyramid) of derived images of progressively coarser resolution, but correspondingly fewer data points. Block cross correlation in the coarsest resolution is computationally fast and builds a crude model of the displacement field of the sea ice. This crude model is used to guide searches in the pyramid of progressively higher resolution images. As one moves down the pyramid to the highest resolution image, searches are guided from previous results and the displacement field is continually refined.

The second technique corresponds more closely to the manual (visual) technique. Distinctive features are located in the reference (initial) image and then located again in the test (subsequent) image. This is a pattern recognition problem where techniques are dependent upon the image content. For our features we use segments of lead-floe boundaries. Thus each image becomes a set of boundary segment features. The set of

Proceedings of IGARSS' 86 Symposium, Zürich, 8–11 Sept. 1986. Ref. ESA SP-254 (published by ESA Publications Division, August 1986).

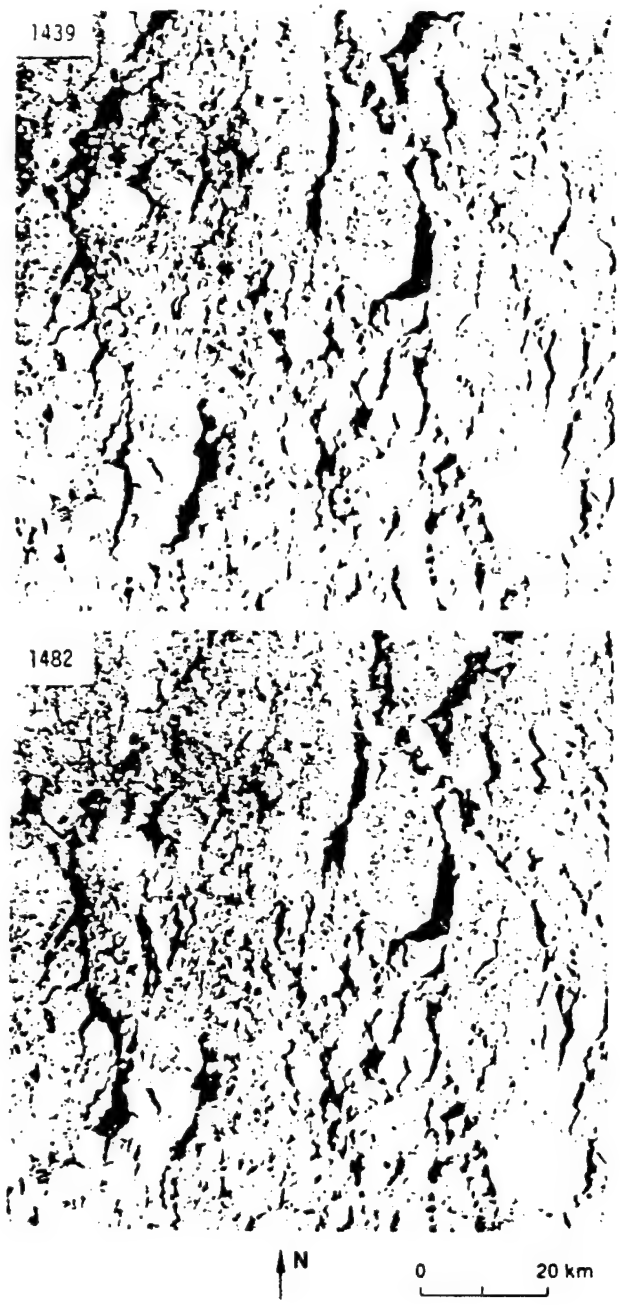

Figure 1. Two SEASAT SAR images of the same area collected over the Beaufort Sea three days apart on orbits 1439 & 1482.

features in the reference image forms the tie points which are then located in the test image and used to derive the ice displacement (velocity) field.

2. SEA ICE TRACKING BY IMAGE PYRAMIDS

2.1 Pyramid Correlation

The problem of tracking sea ice from two radar images can be solved by finding a correspondence between the two images at points which represent the same scene, i.e. the same sea ice image. Cross-correlation of blocks of pixels in the images can be used to find matching scene points in the images. The displacement vector between matching points is taken to be between block centers with the largest correlation coefficients. This displacement information, together with the times of acquisition of the images, can be used to derive velocity information.

Correlation is one of the most expensive image processing algorithms. One way to speed up the computation is to apply the correlation to an image pyramid data structure (see section 1). Pyramids are constructed for each of the two images and then the following algorithm is used:

1. For each non-overlapping block of size (I x I) in the coarsest level of Pyramid 1, calculate a displacement vector by finding the global max of the correlation with the coarsest level of Pyramid 2

2. For each finer resolution level of the pyramid do the following:

   A. Filter the displacement vector field for the previous (coarser) pyramid level in order to remove gross errors.

   B. Interpolate the displacement vector field calculated at the previous pyramid level to provide displacement estimates for each (I x I) non-overlapping block of the current level of Pyramid 1.

   C. For each (I x I) non-overlapping block of the current level of Pyramid 1 find the local max of the correlation with the current level of Pyramid 2 by searching in a (M x M) window centered at the displacement estimate of the current level of Pyramid 2.

3. Optional: Remove displacement vectors with the lowest confidence measure.

The algorithm starts at the top, coarsest pyramid level and proceeds 'top-down' a level at a time. At the coarsest level, the area to be searched in the second image is not constrained. It is important to filter gross errors in the displacement vector field because errors in the top levels of the pyramid propagate to the lower levels. The displacement vector field is then interpolated between pyramid levels since an estimate is needed for those blocks for which there is no computed displacement at the coarser level. At each level in the pyramid, the estimated location of the largest correlation found at the previous, coarser pyramid level constrains the locations searched at the current pyramid level. These location constraints decrease the total number of locations that must be searched.

2.2 Experiments with SAR ice images

The two SEASAT images of sea ice in Fig. 1 were used in the pyramid correlation experiments. The images were first averaged in 10 x 10 blocks to create 384 x 384 pixel images. The averaged images were then histogram equalized. Pyramids with three levels were created from both images by using a lowpass filter with a gaussian transfer function and resampling. The resulting levels of the pyramids had 96 x 96, 192 x 192 and 384 x 384 pixels.

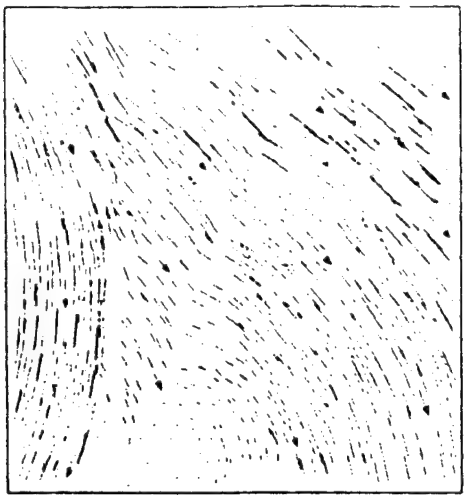

Figure 2. Sea ice velocity field obtained by manual tracking of Fig. 1 images.

The particular implementation of the above pyramid correlation algorithm used 16 x 16 blocks and 32 x 32 search windows at the two finer resolutions. This resulted in 170 times fewer calculations than direct correlation. The correlation measure used in all the experiments was the variance normalized cross-correlation coefficient. We experimented with various methods of filtering the displacement vector field in order to remove gross errors. The smoothing filter that provided the best results was a magnitude median filter where each displacement vector was replaced by the vector in its 8 point neighborhood with the median magnitude. This filtering method successfully removed displacements with errors in magnitude, but did not perform well at points with errors in displacement direction. For the images used, this was not a major problem. We also tried two different interpolation methods, a nearest neighbor interpolator and a bilinear interpolator. The bilinear interpolator performed best and required little added complexity.

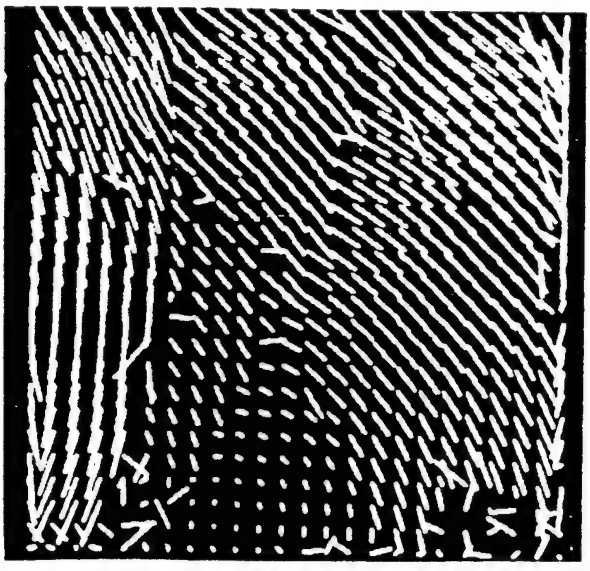

Figure 3. Ice displacement vectors generated by the image pyramid technique.

The experiment using lowpass pyramids with the median filter and the bilinear interpolation gave the best results. Figure 3 shows the displacement vectors at the 384 x 384 resolution. The direction of most vectors is from top to bottom. Comparing these displacement vectors with the manually generated vectors in Figure 2, it is seen that the method performs very well. The problem areas at the edges of the figure correspond to ice features flowing into or out of the finite area covered by the images. Many errors are removed by choosing only those displacement vectors with high correlation coefficients. Fig. 4 shows vectors where the correlation coefficient, $C > 0.4$.

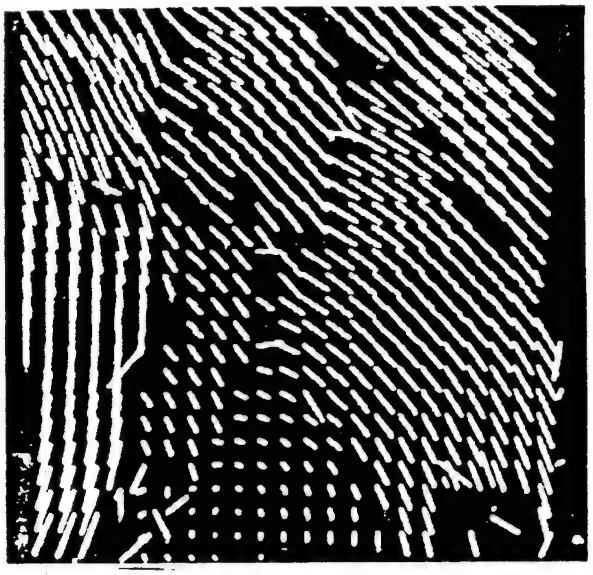

Figure 4. Ice displacement vectors by image pyramid with low confidence vectors removed.

The errors in the interior of the image field cause more concern. From a qualitative evaluation it seemed that some of these errors occurred near leads, where the shapes of ice features change so much that the correlation maximum shifts to some erroneous location. One of the errors occurred in the middle of an ice field which had very little structure, and thus resulted in a broad correlation peak. We assume that this peak was swamped out by noise or systematic distortions such as rotation.

2.3 Discussion

The properties of the pyramid correlation algorithm make it well suited to automatic tracking of ice floes. The search originally takes place at a coarse, global level. This is analogous to people scanning the images to find a general match. The search at the finer levels is analogous to people focusing their attention to specific areas for a more accurate match. The algorithm provides noise immunity by starting the search at the coarse level, where averaging has reduced susceptibility to noise. The constraints at the finer levels provide noise immunity by not allowing a search at all locations. Limiting the search locations lowers the probability of detection of a false peak due to noise. Finally, the algorithm is much more efficient than direct correlation.

The correlation measure currently used cannot detect features which undergo large rotations. This may be alleviated by using a rotationally invariant measure currently being developed.

3. SEA ICE TRACKING USING FLOE-LEAD BOUNDARY FEATURES

3.1 Introduction to the approach

The second sea ice tracking algorithm is a pattern recognition approach. Here we have chosen floe-lead bounary segments as our physical feature. The movement of these features from one image to the next provides the information from which the sea ice velocity field is estimated. Feature patterns must be very distinctive, if not unique, objects. They are characterized by information which is independent of the object location and orientation, though this latter information is, of course, attached to them.

Thus each image becomes a set of features described by parameters independent of the feature location and orientation. The collection of several hundred features, each described by several hundred numbers, reduces the information needed to characterize a 100 X 100 km image. The search space is correspondingly reduced.

Once a feature pattern is recognized in a pair of images, sea ice velocity information can be derived. Since we know something of a feature's physical characteristics, we can derive not just one but many velocity vectors, knowing the displacement and rotation of a particular feature. That is, we know the movement of every pixel in the feature. The results reported here are intended as a progress report on this pattern recognition approach to sea ice tracking. Refinement of the technique is in progress.

3.2 Pattern recognition tracking with floe lead boundary segments

We first present the boundary segment tracking algorithm in outline form.

1. SAR ice field images averaged to obtain 250 x 250 m pixels.
2. SAR image transformed into binary (ice or lead) image by thresholding.
3. Edge detection algorithm transforms image into pattern of floe-lead boundaries.
4. Boundary pixels classified according to surroundings.
5. Boundary segments assembled from classified pixels such that segment corresponds to only one side of a lead.
6. Segments characterized by deviation from straight line fit.
7. Most distinctive features in reference image are searched for in test image to give initial estimate of ice movement.
8. Initial estimate of ice velocity field guides search for less distinct features.
9. Each segment successfully found in test image yields many ice velocity vectors.

3.3 Description of the algorithm

Since SAR pixels cannot be geographically located better than about 200 m and this accuracy is adequate for scientific and practical applications, we average 10 x 10 SAR pixel blocks to obtain an image with about 250 m resolution. This reduces computation time and SAR speckle noise.

Under many circumstances ice and water in SAR image can be distinguished by a simple pixel-intensity threshold (Ref. 4). We use such a threshold to reduce the SAR image to binary pixels, 1 for floe ice and 0 for lead water (including grease ice). Floe-lead boundary edges are identified by simply finding water pixels adjacent to ice pixels.

Next the water edge pixels identified above are classified into eight types according to their surroundings to determine the orientation of the floe-lead boundary edge. The four nearest neighbor pixels are considered to find if there is water above, below, to right or to left of a given boundary pixel. This scheme is illustrated below.

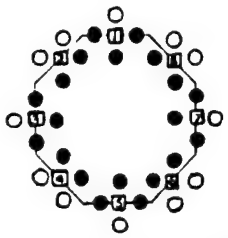

Figure 5. Diagram illustrating edge pixel classification scheme.

The classified pixels are then assembled into boundary segments. The assembly scheme used here begins by finding the dominant direction. For the orbit 1439 image the statistics for edge pixel direction clearly indicated that the dominant lead direction is north-south, and similarly for the 1482 image. Consequently we divided our boundary segments into two groups corresponding to the left and right edges of the leads, to wit:

Left edges (types 2,3,4 and associated 1 & 5)
Right edges (types 6,7,8 and associated 1 & 5)

Our aim here is to match left edges in image 1439 with left edges in image 1482 and, independently, right edges in the image pair. This allows ice floes along the left side of a lead to slip with respect to ice floes along the right side. Thus shear motion, expected across leads, is built into the algorithm.

Boundary segment features are characterized by their deviation from a straight line. First, a "least squares" criterion straight line is fit to a given boundary segment. The distance from this straight line to the segment is calculated at regular intervals along the straight line. This set of deviations characterizes the shape of a boundary segment as illustrated below. Note that this method of characterizing a boundary segment feature is invariant under rotation of the feature.

Figure 6. Edge segment fitted by straight line and characterized by deviation from line.

Recognition of matching feature patterns is done simply by comparing the set of deviation measurements for two candidate features. A variance normalized, cross correlation coefficient (C) was used to evaluate how closely two candidate features

matched. Often segments which we want to compare are of different lengths because of partial break-up of a feature between two successive SAR images. So in our search we include features which are of differing lengths. The shorter feature is slid along the longer feature and C is calculated for all placements of the smaller feature with respect to the larger. This allows for large features to break into parts and still be found.

We have at this point two images which each contain two sets of boundary segment features - left and right edges. The search procedure must select a feature from the reference image (first in time) and try to match it to a feature in the test image (later in time). A successful match reveals ice velocity vectors all along the matching segments.

The search and matching procedure begins by considering only the larger edge features. These features are more likely to be correctly matched and because of the large size reveal the ice velocity field, $\vec{V}(x,y)$, over a large region. For a left edge feature with n pixels we search over left edge features having lengths from $n/2$ to $2n$ pixels. The search is restricted in area to displacements less than 60 km - corresponding to a maximum ice movement of 20 km per day over the three days between the 1439 and 1482 images.

Correct matches for both the sets of left and right edges give two sets of ice displacement vectors. To eliminate erroneous matches we disregard velocity vectors which do not come reasonably close to their neighbors in both magnitude and direction. This set of matches between large features yields an initial estimate of the ice velocity field which can then be used to guide the search for matches between shorter features. Successful identification of a feature in both the reference and test images yields much ice velocity information. Since a feature is generally some tens to even hundreds of pixels in length, many ice velocity vectors can be derived by displacement of each pixel in the shorter of the matching pair of features.

3.4 Application to SEASAT SAR images in the Beaufort Sea

We now apply the boundary segment algorithm to the images of Fig. 1. Since the algorithm is still being developed, the results presented here are only for a first pass through the image data. Boundary edges constructed from the images of Fig. 1 varied in length from 4 to 163 pixels. For this first pass we considered only the longer edges. Thus in the reference image (orbit 1439) edges of 30 or more pixels were used. In the test image (orbit 1482) matching segments of length $(n/2) = (30/2) = 15$ pixels and above were considered. The resulting sets of boundary segments for the orbit 1439 and 1482 images are shown below.

Each 1439 edge was compared to the set of 1482 edges seeking the best match by maximizing C. The search was restricted to edges within 60 km of the 1439 edge location since ice movement of over 20 km/day is unlikely. After the displacement vectors (between segment centers) were calculated for matching left edges in the two images, this process was repeated independently for right edges. Only then were results compared.

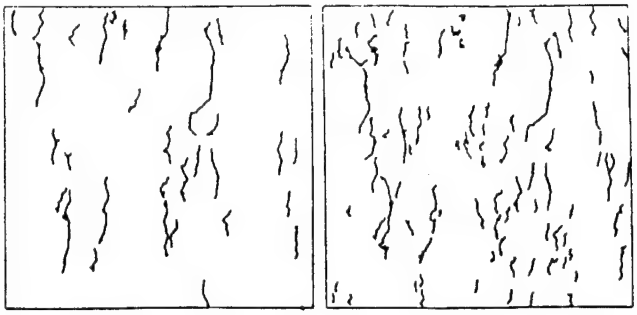

Figure 7. Long boundary segments constructed from orbit 1439 (left) and orbit 1482 (right) SAR image data.

On this first pass through the data we want to insure that only correct displacement vectors are selected. Thus we demanded rather strict agreement between neighboring displacement vectors. We thus assumed that, for a small area of the image, the correct left and right (edge) displacement vectors should not vary in length by more than 30% or have an angular deviation greater than 10 degrees. Only those left edge displacement vectors for which a similar right edge displacement vector could be found within 15 km were recorded. Although this constraint eliminated a few correct displacements, it also eliminated many erroneous displacements arising from correlations between nearly straight edges.

Fig. 8 below shows the displacement vectors for the centers of the matched boundary segments. Each of the vectors represents a family of displacement vectors resulting from the known displacement of each pixel in the segment pair. A more dense and extended field of ice displacement vectors is thus summarized by these few vectors.

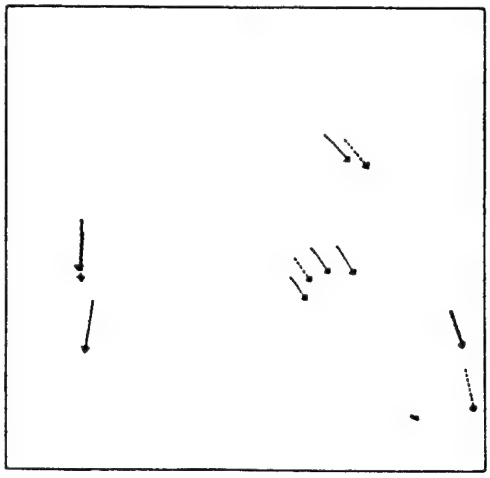

Figure 8. Ice displacement (velocity) vectors from matching of long boundary segments in images 1439 and 1482. Solid lines are left edges and dotted lines right edges.

These displacement vectors agree well with the manually generated vectors of Fig. 2 and the image pyramid generated vectors of Figs. 3 and 4. From these initial results it is clear that successive passes will have to be made through the data. The

displacement vectors calculated on this first pass can be used to narrow the search area on subsequent passes with the goal of finally calculating a displacement vector for a majority of the edges. Other distinctive sea ice features such as pressure ridges could also be used in feature tracking just as the boundary segments are here.

4. COMPARISON OF METHODS

Given our results, we can qualitatively address some of the advantages and disadvantages of the above techniques. In particular, we can compare the methods using an outline suggested by Kashef and Sawchuck (Ref. 5).

A feature-matching method, such as 'boundary segment,' approaches map (image) data differently from a correlation method, such as 'image pyramid.' Whereas correlation methods rely on the intensity values of map data, feature-matching methods rely on detected edges, boundaries, and vertices of map data. The advantage of using 'boundary segment' in tracking sea ice lies in reducing an image of millions of pixels to one of thousands of pixels. Only relevant data applies to tracking. The potential cost-savings for computational speed exist, depending on how 'relevant' the reduced data is. In particular, one should only pick those edges, boundaries, and vertices common to both images for tracking.

Picking those edges, boundaries, and vertices common to both images remains difficult. Thus, the advantage for 'boundary segment' also harbors a disadvantage. Boundaries may fragment, rotate or disappear. Furthermore, detectable boundaries may depict more than one floe, thereby compounding the tracking problem. Hence, the disadvantage to 'boundary segment' is the difficulty in identifying those edges, boundaries, and vertices common to both images.

Correlation methods surmount this difficulty by assuming little or nothing about image content. Traditionally computation-intensive, correlation methods become attractive with some of the newer algorithms such as pyramid correlation. As discussed, 'image pyramid' techniques can track sea-ice floes in a manner more efficient than direct correlation. The noise immunity provided by 'image pyramid' techniques comes as an added bonus. Therefore, the advantage of using 'image pyramid' techniques stems threefold: 'image pyramids' assume little about image content; 'image pyramids' can track global displacements well; 'image pyramids' have inherent noise immunity.

Despite the advantages of using 'image pyramid' techniques, 'image pyramid' techniques like the one currently used for this research cannot detect small-scale pattern changes which involve a large rotation. This problem is significant given the rotational, translational, nature of sea ice.

To address this drawback, one can opt for two schemes. One scheme involves substituting a rotation-invariant measure in place of standard correlation. Another scheme synthesizes a hybrid method from feature-tracking and correlation. For example, the feature-matching method presented here is conditioned to small-scale rotation changes. A synthesis of feature-tracking and correlation methods seems likely in the future.

5. SUMMARY AND CONCLUSIONS

Below we summarize major results and conclusions. Significant further research is needed to produce an efficient and reliable algorithm for automatically extracting the sea ice velocity field from SAR image data.

1. Estimates of the sea ice velocity field are successfully derived from SAR images using the image pyramid (hierarchical correlation) technique.

2. Further refinement of the image pyramid technique should include removal of a small number of erroneous velocity vectors using constraints dependent on correlation coefficient, near neighbor velocities, velocity gradients, etc.

3. Estimates of sea ice velocity are successfully obtained over limited areas using the boundary segment tracking technique.

4. Further refinement of the feature tracking technique should include use of pressure ridge features, constrained search and relaxation techniques.

6. ACKNOWLEDGEMENTS

We gratefully acknowledge image data supplied by Dr. Frank Carsey at Jet Propulsion Lab. We are also grateful for financial support from NASA Oceanic Processes (Drs. Robert Thomas and Ken Jezek) and Office of Naval Research (Code 422 RS, Dr. Charles Luther)

7. REFERENCES

1. Weller G et al. 1983, Science Program for an Imaging Radar Receiving Station in Alaska, NASA Jet Propulsion Lab., Pasadena, CA.

2. Carsey F, Curlander J, Holt B & Hussey K 1983, "Shear Zone Ice Deformation Using Supervised Analysis on SEASAT Data," A.I.A.A. 21st Aerospace Sciences Meeting, Reno, Nevada.

3. Curlander J, Holt B & Hussey K 1985, Determination of Sea Ice Motion Using Digital SAR Imagery, I.E.E.E. J. Ocean Engr. (in press).

4. Fily M & Rothrock D 1985, "Extracting Sea Ice Data from Satellite SAR Imagery," IGARSS '85, Amherst, MA.

5. Kasef & Sawchuck A 1982, "A Survey of New Techniques for Image Registration and Mapping," Applications of Digital Image Processing VI. Proceedings of the S.P.I.E., San Diego, CA.

OBSERVING ROTATION AND DEFORMATION OF SEA ICE WITH SYNTHETIC APERTURE RADAR

J.F. Vesecky, R. Samadani, J.M. Daida, M.P. Smith, and R.N. Bracewell

STAR Laboratory, Electrical Engineering Department
Stanford University, Stanford CA 94305-4055

ABSTRACT

Synthetic aperture radar (SAR) provides an excellent means of observing the movement and distortion of sea ice over large temporal and spatial scales. SAR observations are not affected by clouds or lack of sunlight. The European Space Agency's ERS-1 satellite as well as others planned to follow will carry SAR's over the polar regions beginning in 1989. A key component in utilization of these SAR data is an automated scheme for extracting the sea ice velocity field from a sequence of SAR images of the same geographical region. Several schemes are considered. The image pyramid area correlation (IPAC) method, also known as hierarchical correlation, has successfully performed automated sea ice tracking, but is vulnerable to uncertainties if the ice rotates more than about 10° to 15° between SAR observations. Since ice motion is not uniform, window size is important during cross correlation operations. Selection of optimum window size depends on requirements regarding accuracy of location and suppression of spurious sidelobes. Rotation–invariant methods have the potential to succesfully track isolated floes in the marginal ice zone and may also be helpful in cases of rotating pack ice. Hu's invariant moments are considered as a possible candidate for rotation-invariant tracking. Feature tracking is inherently robust with respect to tracking rotating sea ice, but has some limitations when floe-lead boundaries are used as features. The use of pressure ridge features is indicated. It appears that an automated sea ice tracking algorithm will need a variety of techniques to operate successfully over a wide range of sea ice conditions.

Keywords: Sea ice, synthetic aperture radar (SAR), automated tracking, rotation, image pyramid, feature tracking, invariant moments

I. INTRODUCTION

Sea ice remote sensing is important because of the high spatial and temporal variability of sea ice, its wide geographic extent and its impact on weather, climate, arctic off-shore engineering, transportation and military operations. Sea ice dramatically changes the air-sea energy balance and energy transport. Since sea ice covers significant and variable areas of the Arctic and Southern Oceans, it has a significant impact on both polar and global weather and climate.

The high variability of sea ice coupled with its large extent makes remote sensing techniques a necessity for large-scale ice science as well as for timely practical applications, such as deployment of ocean drilling platforms. Since polar regions are often cloud covered and/or without sunlight for long periods, the ability of synthetic aperture radar (SAR) to provide large scale, high resolution images through clouds and without sunlight gives it a central role in sea ice remote sensing. SAR provides good information on sea ice extent, movement and deformation, internal geometry (structure of floes and leads) and surface roughness [1]. Some useful information on sea ice types, thickness, and physical properties, can also be obtained from SAR images. Examples of SAR images of sea ice are given in Fig. 1 below and by Weller et al. [1].

The process of retrieving ice motion information from a sequence of SAR images (of the same geographic area) revolves around two principal items, namely:

1. Identifying regions in a sea ice field to use as 'tie points' for ice floe tracking.
2. Finding the same tie points in subsequent images of the sequence.

Once ice displacement is known, ice velocity can easily be calculated since the elapsed time between the SAR images is known. In this paper we shall consider the ice velocity and displacement fields as equivalent since they are simply related by a scale factor.

The tracking process has been accomplished manually using a split-screen video display and an experienced operator. Ice velocity is computed automatically once the locations of tie points are marked in a pair of images on the screen. Thorndike & Rothrock [1] have produced interesting results using this technique; further work has been done by Carsey et al. [2] and by Curlander, Holt and Hussey [3]. However, this process is too slow and expensive for real time and/or extensive

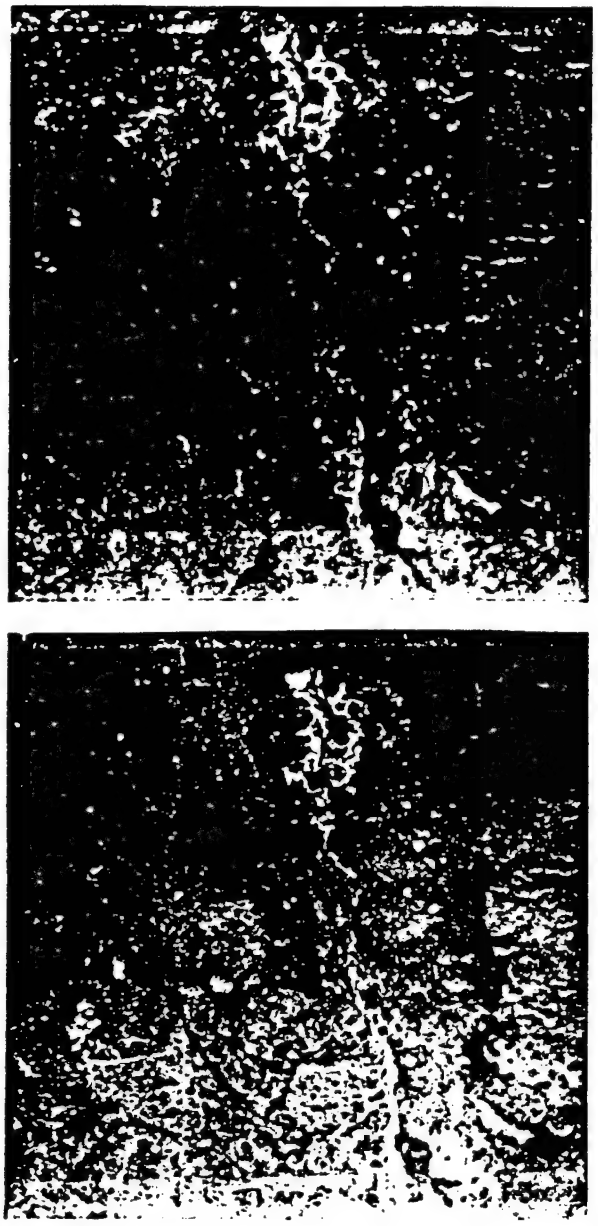

Fig. 1. A pair of co-spatial SEASAT SAR images of sea ice in the Beaufort Sea from orbits 1396A (top) and 1439D (bottom), collected on October 2 and October 5, 1978. Banks Island lies along the right edge of the images.

analysis of images provided by long-term satellite SARs. Two and possibly three such satellite SARs are scheduled to be in orbit by the early 1990s, namely the European ERS-1, the Japanese ERS-1 and the joint Canadian / U.S.A. RADARSAT. Real aperture radar images at low resolution are apparently also available from the Soviet Kosmos 1500 series satellites. Hence, the development of automated techniques is a primary requirement for successful use of satellite or aircraft SAR images in sea ice remote sensing.

Automated ice tracking algorithms have been developed which work reasonably well in regions where there is little rotation and distortion, e.g. in portions of central pack ice [4 and 5]. However in regions where there is significant ice rotation, greater than 10° to 15°, the existing image pyramid area correlation, IPAC, (also called hierarchical correlation) methods are not expected to work well because the cross correlation comparisons are made between image blocks which have been translated in position, but not rotated. For a much used image pair (SEASAT orbits1439 and 1482) upon which the image pyramid algorithm works well, the maximum ice rotation is some 5°. Recent work by Vesecky et al. [6] has shown that ice motion containing shear and distortion can also cause errors when using image pyramid methods.

In this paper we discuss the impact of ice rotation and distortion on sea ice tracking algorithms and report several new results concerning the performance of existing algorithms and methods for improving tracking performance when significant ice rotation and distortion are present. In section 2, we discuss the effects of rotation and distortion on the IPAC algorithm. In this section we report measurements of block cross-correlation function variations with respect to rotation angle and shear angle. The effects of window size on cross correlation between image pairs are also discussed. In section 3, we consider the use of rotational invariant measures to overcome the vulnerability of the IPAC method to ice rotation. This method is applied to ice floes which have rotated during the time interval between collection of the members of an image pair. A case study using SAR images from SEASAT orbits 1438 and 1481 is examined. In section 4, we discuss briefly the advantages, and some limitations, of using our feature tracking algorithm [5,6] to track rotating ice fields. We summarize our conclusions in section 5.

2. SENSITIVITY OF BLOCK CORRELATION TO SEA ICE ROTATION AND DISTORTION

Block correlation for matching in a pyramid data structure has been applied to SEASAT sea ice scenes [4,5,6]. We have sectioned pairs of SAR images of the same geographic location into non-overlapping image pairs. The IPAC algorithm has been successfully applied in these pack ice regions. It has also performed successfully on the pair 1439 and 1482 taken as a whole.

Pure translational motion is the strict assumption one makes when the correlation coefficient is used as a similarity measure between images. Since pack ice regions are observed to move as large blocks, approximating rigid translation, we believe that IPAC will sucessfully track these regions. Here we assess the performance of the algorithm in the presence of rotation and non-rigid motions. These types of motion are expected in the marginal ice zone.

The study of the degradation of the correlation coefficient due to geometric distortions is important for two reasons. First, it can be used to determine the applicability of correlation when the motion is not strictly translation. Second, it can be used to set suitable

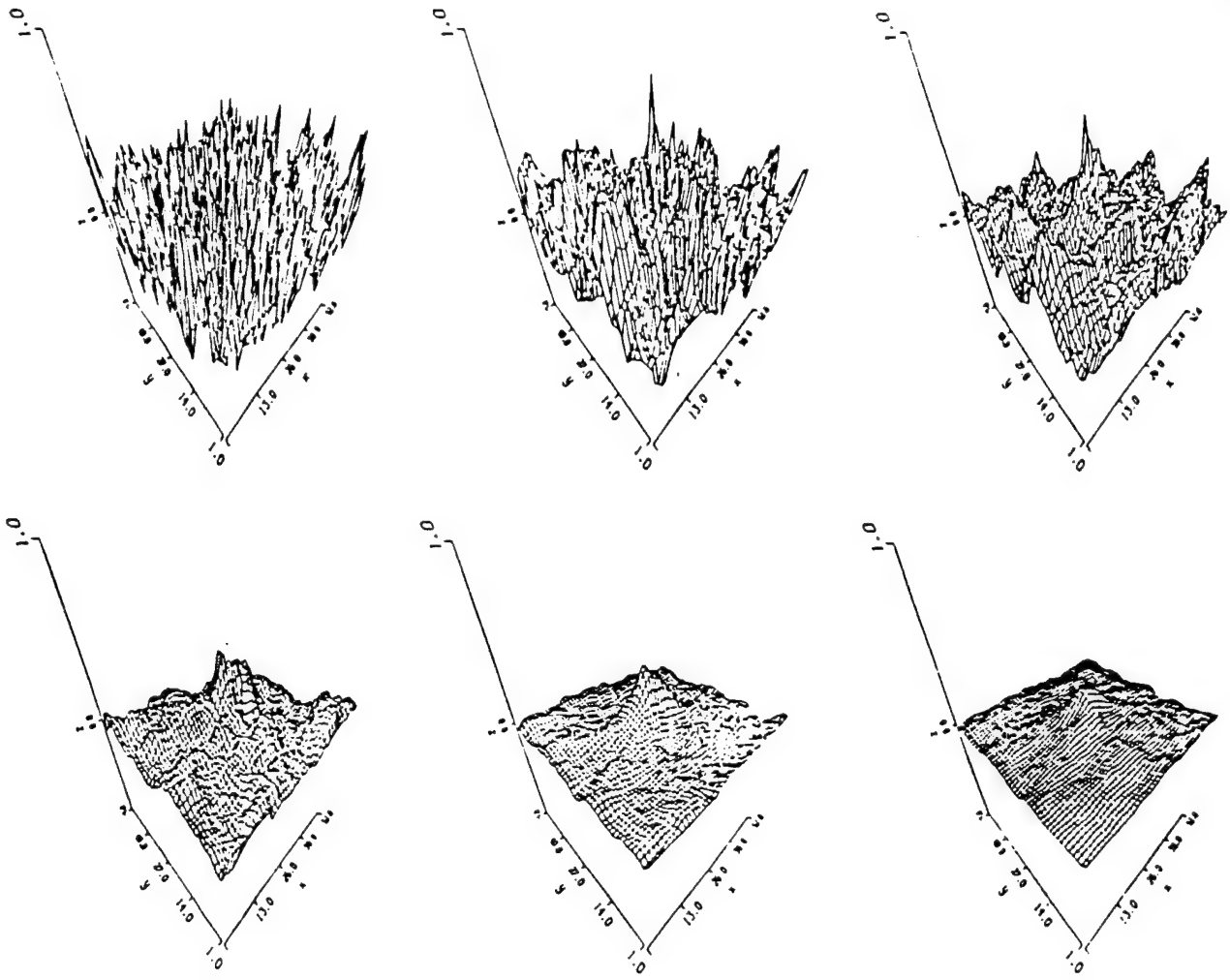

Fig. 2. Perspective plots of the two dimensional cross-correlation function between matching SAR sea ice scenes from SEASAR orbits 1439 and 1482. Image resolution was averaged to 250 meters. The window size is increases in steps of a factor 2 moving from left to right: i.e. window sizes are 5, 9, 17, 33, 65, and 129 pixels to a side.

correlation window sizes.

It is known that the linear correlation coefficient is affected by noise and by geometric distortions [7]. The noise considerations apply to all applications of correlation, including registration, where it is most commonly used. Our application, however, is to motion detection and the geometric distortions that occur are basically the result of nonuniform motion and are an expected occurrence. In this section we present results related mainly to geometric distortions.

The analysis of the degradation of correlation coefficient due to geometric distortions is complex and, unfortunately, data dependent. For this reason, we have conducted an experimental appraisal of distortion effects on real ice data.

2.1 Scale of the Motion

If the motion between the two images is pure translation, then one can in principle find the motion by cross-correlating the two images. In statistical terms, the problem is to find an estimator for the translation. In order to find a minimum variance estimator, given noisy data, one would use all the data one has and this results in chosing the largest window possible.

If the motion between the two images is not a pure translation, then there is a tradeoff involved in picking a window size for correlation. Larger windows are desired for accuracy in the estimators, but are undesirable for scales of motion smaller than the window size. Smaller windows, on the other hand, are desirable if the motion is only locally uniform but are undesirable for accuracy of the estimators, especially in the presence of noise.

We show in Figure 2 a sequence of perspective plots of the cross correlation of a matching section of 1439 and 1482 which were averaged to 250 meter pixels. From left to right in the figure, the window size is increased by a factor of about two at each step. At small window sizes, the cross-correlation is evidently noisy and may result in misses if a large enough region is searched for a match. We find the window size 17x17 to have a distinct peak and it is, therefore, suitable for use. The larger window sizes show a decrease in correlation coefficient. We

observe nonuniform motion in this region of the images and we attribute the decrease in the correlation coefficient to this non-uniformity. Although the peak for these larger window sizes may be easily extracted, it would not represent the motion accurately.

V. E. Borodachev [8] has studied aerial photographs and has found the average size of unfractured ice to be 10 kilometers. This is about the size of the 16x16 windows we currently use and further justifies the window size if we assume that one or two ice blocks move uniformly.

2.2 Rotation and Shear

We have studied the effect of rotation and shear by simulating distortions on the computer. We are able to remap an image by specifying any linear transformation between the coordinates of the original image and the output image and then using bicubic interpolation to resample the image. In particular, we can simulate rotation and pure shear using the following matrices:

Rotation

$$\begin{pmatrix} \cos\theta & -\sin\theta \\ \sin\theta & \cos\theta \end{pmatrix}$$

Shear

$$\begin{pmatrix} 1 & -\tan\theta \\ 0 & 1 \end{pmatrix}$$

Our experimental study consisted of extracting twenty non-overlapping 16x16 subimages at 125 meter pixels of 1439 and 1396 and applying both transformations to each subimage at increments of one degree. We then find the cross-correlation between the original and the distorted image for a window size of 16x16 pixels, which is used in our current implementation of the IPAC algorithm [5,6]. Figure 3 shows a plot of the average correlation coefficient for the twenty subimages as a function of angle of rotation or angle of shear, as defined by the matrices above.

If the correlation coefficient of the correct match is low, then the probability of a mismatch increases. In one case, when we searched a local area around the correct match, we found a higher correlation coefficient than the correct one when the rotation angle was 16 degrees. The maximum correlation coefficient was .39 and the distance to the correct match was about 3 pixels. We believe that rotations of ten degrees will not hamper detection by block correlation.

One can intuitively interpret the fact that the shear curve lies above the rotation curved by considering the overlap of pixels for a given shear or rotation. The pixels in the middle row of the image are fixed for a shear whereas only the middle pixel is fixed for a rotation.

A further study determines the effect of resolution on rotation effects. Figure 4 shows the effects of rotation on

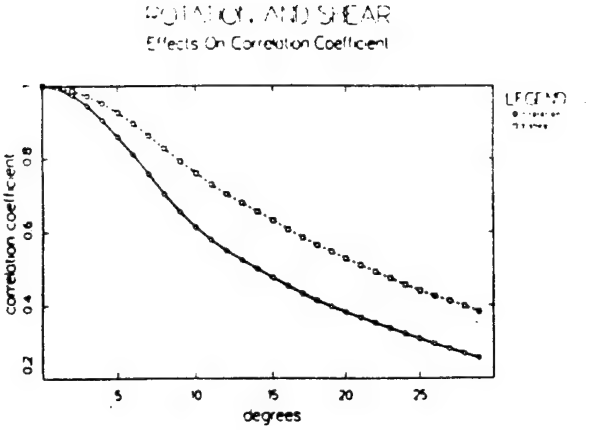

Fig. 3. Averaged two-dimensional cross-correlation function with respect to angle of rotation and angle of shear. Twenty SAR sea ice scenes, extracted from SEASAT orbits 1396 and 1439, were used in the averaging process.

images depicting the same scene at various levels of resolution, corresponding to the pyramid levels used in the current IPAC algorithm. We note that the coarsest level of resolution is more immune to rotation effects than the equivalent window would be at the finest level. This is an advantage of pyramid correlation in areas of rigid rotation.

In summary, correlation is strictly valid only for translational motion. Studies of the actual ice data, as represented by Figure 2, have shown that the ice motion is not translational, but has rotational and nonuniform translational components. We have shown, however, that correlation is still practical under the various distortions studied. Studies of simulations of rotations and shears, as depicted in Figure 3, have shown that correlation is useful, up to moderate angles of distortion. In particular, we believe that rotations of about 10° can be dealt with adequately with correlation. Finally, Figure 4 shows the effect of correlation in a pyramid. As expected, smaller windows, at the coarse level are more immune to rotation that their equivalent windows could be at the fine

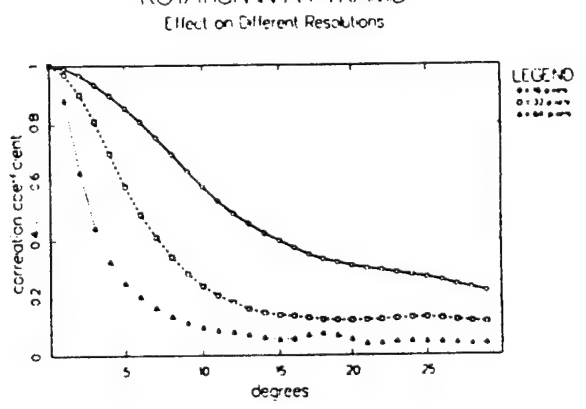

Fig. 4. Two-dimensional cross-correlation function with respect to angle of rotation for window sizes of 16, 32, and 64 pixels to a side all depicting the same area of 16x16 kilometers. Twenty SAR sea ice scenes, extracted from SEASAT orbits 1396 and 1439, were used in the averaging process.

resolution level.

3. APPLICATION OF INVARIANT MOMENTS FOR TRACKING SEA ICE WHICH ROTATES

3.1 Invariant Moments: Background

Invariant moments help solve the problem of identifying objects in a scene that changes because the objects rotate from one image of the scene to the next. As mentioned in the previous section, IPAC will handle rotations in sea ice features up to about 10° to 15°. Beyond that, rotations will start to affect the ability of the algorithm to correctly track features. Rotations of that magnitude or greater commonly occur in places like the marginal ice zone. One way to work around these large rotations is to use a method that ignores rotations in a scene altogether. Invariant moments is one such method, whereby invariant moments reduces a scene to a set of numbers, indices that do not change with rotation.

The problem of matching rotated sea ice features is more complex, however, than the problem of coping with rotational transformations because sea ice features may change with translation or rotation as ice floes move across open water or ice fields. Floes may collide with each other, thereby creating new features. Rotations of floes will affect how features are manifested in a SAR image because SAR is sensitive to the aspect angle from which a scene is viewed [2,3]. Translations of these rotated floes might occur across a changing background of new ice, wind-roughened ocean, or pack ice. A sea ice tracking algorithm is put to task under these conditions.

IPAC methods will handle a significant number of these rotated and translated ice features, as discussed in the previous section. However, not all ice features are amenable to this type of tracking. For example, ice floes in the marginal ice zone commonly rotate many times while drifting across open water. It is for these types of ice features that we consider invariant moments. We think that invariant moments will also be helpful in sorting out ambiguities which arise during application of IPAC algorithms to regions with ice rotation greater than the limits suggested in section 2.

Although a variety of rotation-translation invariant measures exist, we use those given by Hu [9]. These seven indices demonstrate invariance under translation and rotation. Furthermore, they also demonstrate invariance under scaling and optical inversion. Such properties—invariance under translation, rotation, scaling, and mirroring—make these indices well suited for scene matching problems [10]. To show why Hu's invariant moments have these properties, we will highlight their derivation.

Hu's invariant moments start with the theorem stated by Papoulis in 1968. . In essence, this theorem infers that an image represented by a image intensity function $f(x,y)$ bounded in extent can be reduced to a unique sequence of double moments. This means that an image many thousands of pixels large will compact down to a sequence of a few numbers. Note that low-order double moments of images are analogous to moments for objects (mass, center of mass, moments of inertia).

Double moments by themselves show no invariant properties. However, Hu derived invariant moments from double moments with a series of transformations. From double moments, we obtain central moments. Under the translations of coordinates, central moments remain invariant. From central moments, we obtain normalized central moments. Under scaling, in addition to translation, normalized central moments remain invariant. From normalized central moments and with the theory of algebraic invariants, we obtain Hu's indices. Under proper and improper orthogonal rotation and mirroring, in addition to translation and scaling, Hu's indices remain invariant. Finally, since the magnitude of these moments may span many orders, the typical convention is to take the absolute value of the log of Hu's indices.

3.2 Case Study: SEASAT Orbits 1438 and 1481

While in theory, Hu's invariant moments look attractive as an alternative matching algorithm to IPAC methods in tracking some of the more profoundly rotated sea ice features, in practice the invariant moments work less well. A significant problem with Hu's invariant moments has to do with interference from other floes.

To illustrate how Hu's invariant moments work with SAR images of sea ice, we take several examples from the SEASAT image pair from orbits 1438 and 1481. These particular examples come from a marginal ice zone in the Beaufort Sea.

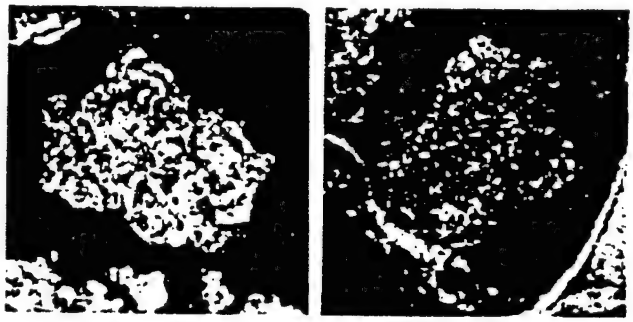

Fig. 5. Example of a rotated ice floe, from the marginal ice zone in the Beaufort Sea. Image resolution was averaged to 250 meters. The window size is 100x100 pixels. a) Reference floe: orbit 1438, October 5, 1978. b) Reference Floe: orbit 1481, October 8, 1978.

Figure 5a depicts an isolated floe (orbit 1438) which will serve as our reference floe. Figure 5b depicts that same floe which has since drifted and rotated (orbit 1481). Rotation of this floe apparently did affect how its features are manifest in a SAR image: the lower end of the floe brightens while the rest of the floe dims with the rotation.

Furthermore, the translation of this floe did occur across a changing background of ice and wind-roughened ocean. The ice floe in 1481 appears in what looks like a thickening background of ice, thereby altering some of the floe's boundaries: the bright lower right hand corner of Figure 5b is interpreted as wind-roughened ocean.

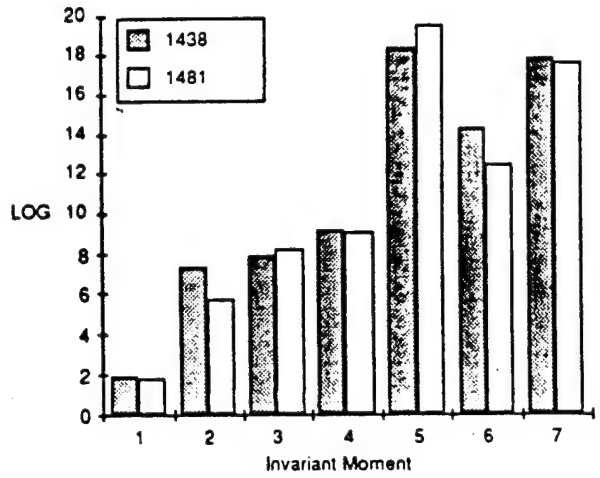

Fig. 6 Histogram of the absolute value of the log of the invariant moments corresponding to the reference floe.

Figure 6 shows a histogram of the invariant moments corresponding to Figure 5. This histogram illustrates two points. The first point is that the invariant moments span about seventeen orders of magnitude, ranging from 10^{-2} to 10^{-19}. This large range of values is common with Hu's invariant moments. In general, the first invariant moment has the lowest order of magnitude, with the order of magnitude increasing with order of invariant moment. The second point is that the invariant moments match well at the first, third, fourth, and seventh moments. As a rough indicator, these matches between invariant moments do point to a correct match between scenes.

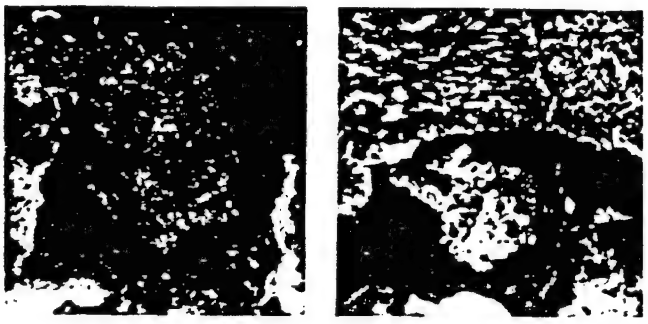

Fig. 7. Others floes from orbit 1481. Image resolution was averaged to 250 meters. The window size is 100x100 pixels. a) Floe A. Invariant moments correctly distinguish between this and the reference floe 1438. b) Floe B. Invariant moments yield ambiguous results between this and the reference floe 1438.

Figure 7 depicts two other floes for comparison. Both floes were taken from 1481. Figures 8 and 9 illustrate how the invariant moments from these floes compare with the invariant moments from the reference floe in 1438.

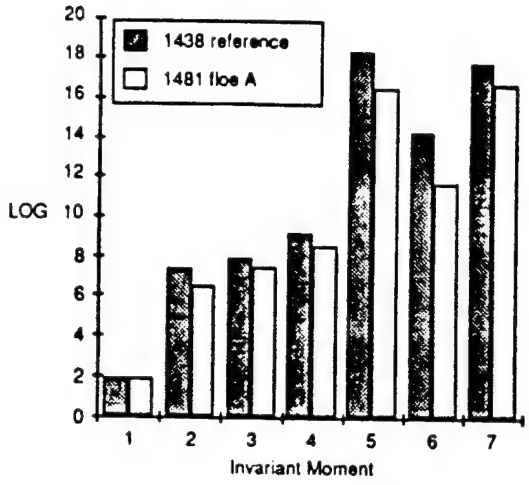

Fig. 8. Histogram of the absolute value of the log of the invariant moments corresponding to Floe A. The invariant moments from the reference floe 1438 are included for comparison. Invariant moments correctly distinguish between this and the reference floe.

Figure 8 illustrates how dissimilar scenes might appear in terms of invariant moments. With the exception of the first invariant moment, all the remaining invariant moments of floe A fell below those of our reference floe. Other dissimilar scenes would have a invariant moment signature different from the reference signature.

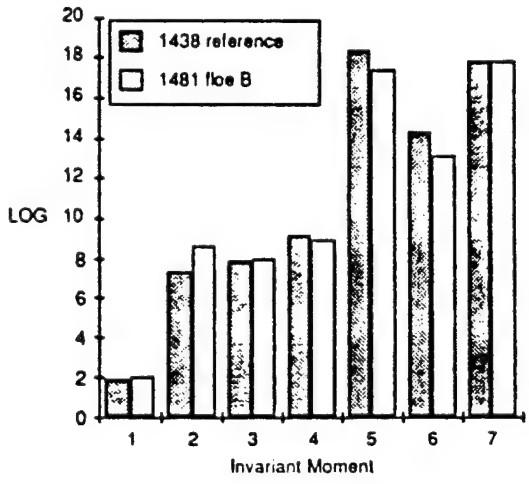

Fig. 9. Histogram of the absolute value of the log of the invariant moments corresponding to Floe B. The invariant moments from the reference floe 1438 are included for comparison. Invariant moments yield ambiguous results between this and the reference floe.

Figure 9 illustrates how ambiguous scenes might appear. Even though the two scenes look dissimilar, the invariant moments of floe B suggest that the reference floe and floe B are matched. This ambiguity could occur when the background, in this case a part of another floe above floe B, interferes with determining a match. This problem would occur with correlation methods as well. Other ambiguities would also occur should a smaller flow look similar to the reference floe: Hu's invariant moments are also scale invariant.

This work in invariant moments illustrates what kind of invariant moment signatures we might get from applying Hu's invariant moments. It also indicates possible sources of ambigous matches. For further work, we need to investigate methods that reduce the likelihood of ambiguous matches. For example, some improvements to invariant moment methods for scene matching problems are given by Goshtasby [11]. Such methods need to be applied to Hu's invariant moments before they can be considered as replacements for block correlation measures.

4. FEATURE TRACKING WHEN SEA ICE ROTATION IS PRESENT

4.1. Introduction to the Method

The feature tracking algorithm approaches the problem of sea ice tracking by relying on selected sea ice features rather than the entire content of the image, as in the IPAC method of section 2. There are a wide variety of features in sea ice which one could track, including pressure ridges, isolated floes, and floe-lead boundaries. Initially we have chosen floe-lead boundaries as the physical feature we will track because they are usually the most prominent, distinct, and high contrast features in SAR images of sea ice. The movement of these features from one image to the next provides the information from which the sea ice velocity field is estimated. Feature patterns must be very distinctive, if not unique, objects.

In the feature tracking method each image is transformed into a set of features described by parameters independent of the feature location and orientation. The collection of several hundred features, each described by several hundred numbers, reduces the information needed to characterize a 100 x 100 km image by roughly two orders of magnitude. The search space is correspondingly reduced. Once a feature pattern is recognized in both members of a pair of images, sea ice displacement and hence velocity information can be derived.

In the following paragraph we outline our feature tracking algorithm; more detailed information is given in [5,6]. Given a pair of SAR images of the same geographic area, each image is first averaged to a resolution of about 250 m. Ice and lead are then classified by a simple intensity threshold and floe-lead boundaries identified. Pixels along floe-lead boundaries are classified and assembled into segments. These boundary segments are characterized and thus form the features which are tracked from one SAR image to another collected three days later. Several tracking passes are made through the collections of features in each image. The high confidence ice displacement estimates, corresponding to high correlation between the characteristics of matching features in the two images, are used to guide the search for other matching features and thus more ice displacement estimates.

4.2 Capabilities of Feature Tracking with Regard to Rotation

The feature tracking algorithm is inherently robust with respect to rotation because the features are characterized with respect to a coordinate system tied to the feature itself and not with respect to geographic or image coordinates. To understand this we consider the characterization process in more detail. After pixels along floe-lead boundaries are classified and assembled into segments these boundary segment features are characterized by their deviation from a straight line. First, a 'least squares' criterion straight line is fit to a given boundary segment. The perpendicular distance from this straight line to the segment is calculated at regular intervals along the straight line. This set of deviations characterizes the shape of a boundary segment as illustrated in Figure 10. This method of characterizing a boundary segment feature is invariant under rotation of the feature. There are limitations, however, as noted in section 4.3.

Recognition of matching features is done simply by comparing the sets of deviation measurements for two candidate features. A variance normalized, cross-correlation coefficient (C) is used to evaluate how closely two candidate features match. Often segments which we want to compare are of different lengths because of partial breakup of a boundary segment over the time interval between images. So in our search we include features of different lengths. During the comparison process we slide the shorter feature along the longer feature with C calculated for all placements of the smaller feature with respect to the larger. This allows for larger segments to break into smaller ones and still be found. A successful match reveals ice displacement.

Because this method of characterizing a boundary segment feature is invariant under rotation of the feature one expects that, in principle, a feature which has undergone rotation will be as easily found as one which has not. In the one pair of SAR sea ice images so far examined [5,6] features were successfully tracked using this algorithm. However, the SAR scenes contained central pack ice and the average rotation of the sea ice was only about 5°.

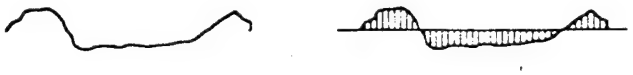

Fig. 10. Boundary segment fitted by a straight line and characterized by deviation from the fitted line.

4.3 Limitations of Feature Tracking with Regard to Rotation

Although our feature tracking algorithm has advantages in terms of following rotating ice, there are also limitations so far as the current algorithm [5,6] is concerned. The limitation arises, not in the characterization of a feature, but in choosing what pixels constitute the feature. Features are constructed by first classifying floe-lead boundary pixels and then assembling them into contiguous sequences of pixels having only certain allowed classifications. The classification system uses surrounding pixels for reference and thus is not completely independent of image coordinates. This process allows two sides of a lead to be separate features and thus move independently, i.e. it allows leads to open and close. Thus the lead-floe boundary surrounding a lead may be chopped into features (for tracking) in two different ways depending on how it is oriented in the first and second images of an image pair.

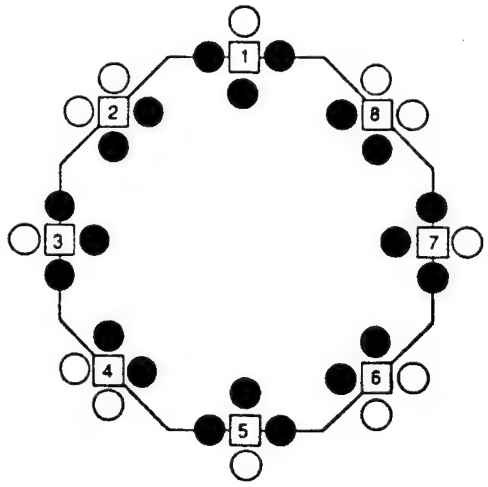

Fig. 11. Diagram illustrating edge pixel classification scheme. The filled circles represent water pixels and the white circles ice pixels.

This problem can be illustrated by considering the diagram of Figure 11. Leads tend to be cracks in ice and thus linear rather than circular. If the majority of the leads in an image are linear, running vertically, then our algorithm [5,6] will assemble edge features as follows:

Left Edges: edge pixel types 2,3,4 and associated types 1 & 5
Right Edges: edge pixel types 6,7,8 and associated types 1 & 5.

If, in the second image of a pair, a particular lead has rotated by say 45°; then some of the pixels making up the left and right edges will be different because a pixel which was type 5 in the first image might become type 4 or 6 in the second image of the pair. Under these circumstances a rotated feature becomes more difficult to track. If the majority of sea ice in a region rotates approximately the same amount, then the algorithm will adapt to the new, dominant, lead direction. Tracking in the presence of rotation should then proceed as in the case of no rotation.

4.4 Improvements of Feature Tracking with Regard to Rotation

Feature tracking is a broad catagory of pattern recognition techniques for application to sea ice. As discussed above, it has inherent advantages for ice tracking in the presence of rotation. We also discussed a limitation which arises from the fact that leads often open and close and thus the dominant edges must be tracked independently. Other sea ice features do not have this limitation. For example, pressure ridge patterns are an evident feature in figure 1 above. Although pressure ridges are less distinct features than lead-floe boundaries, they are more stable since they are not affected by opening and closing of leads. Thus one would expect that incorporating pressure ridge patterns into a feature tracking algorithm would improve performance, particularly in the presence of large and spatially variable ice rotation.

5. CONCLUSIONS

We summarize our major conclusions as follows:

1. The image pyramid area correlation (IPAC) method, also known as hierarchical correlation, has successfully performed automated sea ice tracking; but is vulnerable to uncertainties if the ice rotates more than about 10° to 15° between SAR observations.

2. Window size is important in making block cross-correlation comparisons between SAR images. We find that because ice motion is nonuniform window size choice is a tradeoff between better placement accuracy with smaller windows and lower levels of spurious sidelobe response with larger windows.

3. Rotation invarient correlation methods can successfully track rotating ice floes which are isolated. This technique may also be useful is resolving ambiguities in IPAC displacement estimates which are due to ice rotation (see item 1 above).

4. Feature tracking is inheirantly robust with respect to tracking rotating sea ice, but has some limitations when floe-lead boundaries are used as features. The use of pressure ridge features is indicated.

5. We conclude that an automated sea ice tracking algorithm will need a variety of techniques to operate successfully over a wide range of sea ice conditions.

ACKNOWLEDGEMENTS

We are grateful to Frank Carsey, John Curlander, Ben Holt and Kevin Hussey at the NASA Jet Propulsion Laboratory for supplying sea ice SAR images. Sieglinde Barsch and Stephen Vesecky are acknowledged with thanks for their help in manuscript and figure preparation. We gratefully acknowledge guidance, encouragement and financial support from NASA Oceanic Processes (Ken Jezek and Robert Thomas) and the Office of Naval Research (Charles Luther). We also acknowledge with thanks NASA financial support through the Center for Aeronautics and Space Information Systems, Stanford EECS, NASA grant NAGW 419.

REFERENCES

[1] G. Weller, F. Carsey, B. Holt, D. A. Rothrock and W. F. Weeks, "Science Program for an Imaging Radar Receiving Station in Alaska -- Report of the Science Working Group", NASA - Jet Propulsion Lab., Pasadena, CA, 1983.

[2] F. Carsey, J. Curlander, B. Holt and K. Hussey, "Shear Zone Ice Deformation Using Supervised Analysis on SEASAT Data," *A.I.A.A. 21st Aerospace Science Meeting*, Reno, Nevada, 1983.

[3] J. Curlander, B. Holt and K. Hussey, "Determination of Sea Ice Motion Using Digital SAR Imagery", *I.E.E.E. J. Ocean Engr.*, in press, 1985.

[4] M. Fily and D. A. Rothrock, "Extracting Sea Ice Data from Satellite SAR Imagery," *IEEE Trans. Geosci. & Remote Sensing*, GE-24, 849-854, 1986.

[5] J. Vesecky, R. Samadani, M. P. Smith, J. M. Daida and R. N. Bracewell, "Automated remote sensing of sea ice using synthetic aperture radar", *Proc. IGARSS'86*, 127-132, ESA SP-254, ESA Publications Div., Paris, 1986.

[6] J. Vesecky, R. Samadani, M. P. Smith, J. M. Daida and R. N. Bracewell, "Observation of sea ice dynamics using synthetic aperture radar images: automated analysis", submitted to *IEEE J. Rem. Sensing*, 1987.

[7] H. Mostafavi and F. W. Smith, "Image correlation with geometric distrotion. Part 1: acquisition and performance", *IEEE TRans. Aerosp. Electronic Sys.*, AES-14, 3, May, 1978.

[8] V. E. Borodachev, "The block structure of the ice cover", in *Dynamics of Ice Cover* (L. A. Timokhov, ed.), Oxonian Press, New Delhi, 1984.

[9] M-K. Hu, "Visual Pattern Recognition by Moment Invariants", *IRE Trans. Infor. Th.*, 8,179-187,1962.

[10] R. Wong & E. Hall, "Scene Matching with Invariant Moments", *Comp. Graphics & Image Proces.*, 8, 16-24,1978.

[11] A. Goshtasby, "Template Matching in Rotated Images", *IEEE Trans. Pattern Anal. & Machine Intel.*, PAMI-7, 338-344,1985.

OBSERVATION OF SEA ICE MOTION AND DEFORMATION USING SYNTHETIC APERTURE RADAR: AUTOMATED ANALYSIS ALGORITHMS

J. F. Vesecky, R. Samadani, J. M. Daida, M. P. Smith and R. N. Bracewell

Space, Telecommunications and Radioscience Laboratory
Electrical Engineering Department
Stanford University, Stanford CA 94305-4055

Abstract -- Synthetic aperture radar (SAR) provides an excellent means of observing the movement and distortion of sea ice over large temporal and spatial scales. SAR observations are not affected by clouds or lack of sunlight. The European Space Agency's ERS-1 satellite as well as others planned to follow will carry SARs over the polar regions beginning in 1990. A key component in utilization of these SAR data is an automated scheme for extracting the sea ice velocity field from a time sequence of SAR images of the same geographical region. In this paper we provide an overview of the problem of automated sea ice tracking using SAR images. To begin we briefly describe two basic techniques for automated sea ice tracking: image pyramid area correlation (hierarchical correlation) and feature tracking. Examples of the application of these techniques to SEASAT SAR sea ice images are shown. The results compare well with each other and with manually tracked estimates of the ice velocity field. We note the problems presented to automated tracking algorithms by sea ice which rotates or shears, discussing the dimensions of the problem as well as solutions via the use of rotation invarient correlation and feature tracking. Using the ice velocity field estimated from SAR images one can reconstruct one sea ice image from the other member of the pair. Comparing the reconstructed image with the observed one, errors in the estimated velocity field can be recognized and a useful probable error display created automatically to accompany ice velocity estimates provided to the user. We suggest that this error display may be useful in segmenting the sea ice observed into regions which move as rigid plates and regions of significant ice velocity shear and distortion. We then consider how the several methods discussed can fit together to form a robust algorithm for application to satellite (ERS-1) SAR sea ice data to be collected at the Alaskan SAR FAcility (ASF) at the University of Alaska, Fairbanks. Finally, we discuss the importance of displaying the ice velocity field properly and summarize conclusions.

I. INTRODUCTION

The importance of sea ice remote sensing arises from the high spatial and temporal variability of sea ice, its wide geographic extent and its impact on climate, arctic off-shore engineering, transportation and military operations. Sea ice

dramatically changes the air-sea energy balance and energy transport. Since sea ice can cover significant areas of the Arctic and Southern Oceans, it has an important impact on both polar and global climate.

The high variability of sea ice coupled with its large extent makes remote sensing techniques a necessity for large-scale studies. Since polar regions are often cloud covered and without sunlight for long periods, the ability of synthetic aperture radar (SAR) to provide areally extensive, high resolution images through clouds and without sunlight gives it a central role in sea ice remote sensing. SAR provides good information on sea ice extent, movement and deformation, internal geometry (structure of floes and leads) and surface roughness (Weller, et al., 1983). Some useful information on sea ice types and their physical properties can also be obtained from SAR images.

The process of retrieving motion information from a sequence of SAR images (of the same geographic area) revolves around two principal items, namely:

1. Identifying regions in a sea ice field to use as 'tie points' for ice floe tracking.
2. Finding the same tie points in subsequent images of the sequence.

Once the ice displacement is known the ice velocity can easily be calculated since the elapsed time between the SAR images is known.

This process has been carried out manually on SEASAT SAR data by Thorndike and Rothrock [see Weller et al., 1983] using a split-screen video display and an experienced operator. Ice velocity is computed automatically once the locations of tie points are marked in a pair of images on the screen. Further work on satellite imagry using manual techniques has been done by Carsey et al. (1983) and by Curlander, Holt and Hussey (1987). However, this process is too slow and expensive for real time and/or extensive analysis of images provided by long-term satellite SARs. Two and possibly three such satellite SARs are scheduled to be in orbit by the 1990s, namely the European Space Agency ERS-1, the Japanese ERS-1 and the joint Canadian-US-UK RADARSAT. Real aperture radar images at low resolution are apparently available from the Soviet Kosmos 1500 series satellites. Hence, the development of automated techniques for sea ice tracking is a primary requirement for successful use of satellite SAR images in sea ice research.

In this paper we present an overview of the ice tracking problem, discussing the several component methods used in automated sea ice tracking, detection of errors, the structure of composite algorithms for ice tracking under a wide range of sea ice conditions and finally the display of sea ice velocity field estimates. Sections II, III and IV cover image pyramid area correlation and feature tracking methods as well as methods for coping with situations in which the sea ice rotates between observations. Section V discusses the important problem of error detection using an image reconstruction method. The synthesis of a composite algorithm is covered in section VI. Section VII deals with the display of velocity field results so as to aid the user with interpretation. Conclusions are presented in section VIII.

II. IMAGE PYRAMID AREA CORRELATION METHOD

A. Description of Method

This method, also known as 'hierarchical correlation' or 'nested correlation', comes from the field of pattern recognition and was first applied to the tracking of sea ice by Fily and Rothrock (1986). Cross-correlation of small blocks of pixels from a pair of cospatial images is used to find matching scene points. This is made computationally efficient by first building from each primary, high resolution image a sequence (pyramid) of derived images of progressively coarser resolution, but correspondingly fewer data points. Such a pair of image pyramids is shown in Fig. 1. Block cross correlation in the coarsest resolution images of the pyramid is computationally fast and builds a crude model of the displacement field of the sea ice. This crude model is then used to guide searches in the pyramid of progressively higher resolution images. As one moves down the pyramid to the highest resolution image, searches are guided from previous results and the displacement field is continually refined.

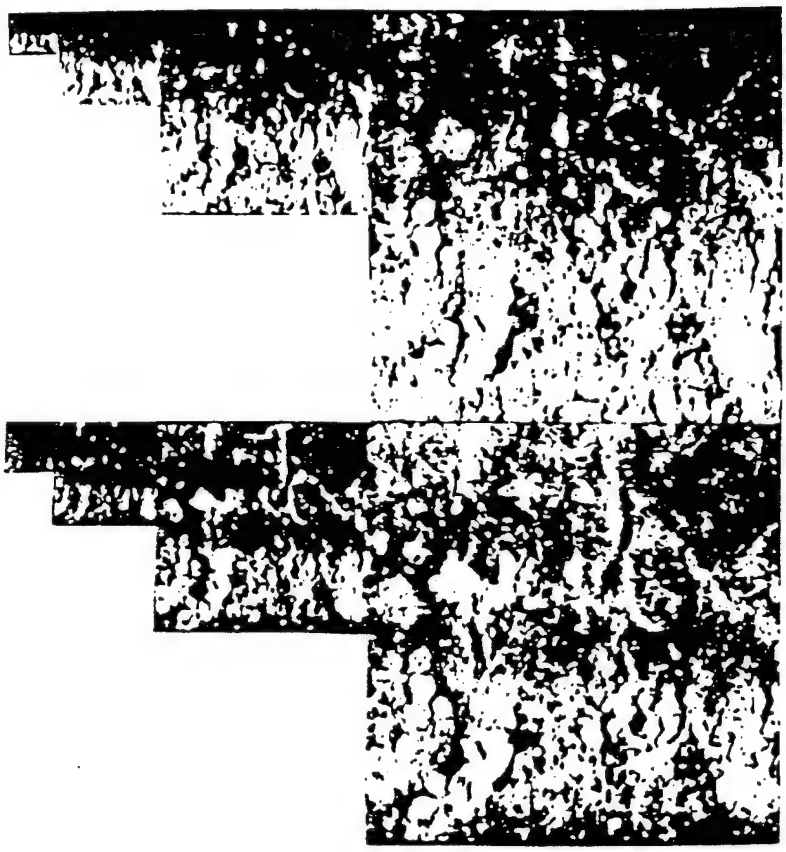

Fig. 1. Image pyramids for two SEASAT SAR images of the same central pack ice area in the Beaufort Sea. The images were collected three days apart on Oct. 5 (top) & 8 (bottom), 1978 on Seasat orbits 1439 and 1482, respectively.

An image pyramid, as shown in Fig. 1, can be viewed as a set of images in a stack. At the bottom of the stack is the original image and at each of the following levels of the stack is a lower resolution image derived from the level below it by first applying a low pass filter and then resampling the image. The result is a pyramid in which, as one traverses from bottom to top, the number of pixels in the images decreases geometrically.

The following steps are needed for effective correlation in a pyramid structure. To begin, pyramids (1, first in time and 2, second in time) are constructed as in Fig. 1; one for each of the two images. Then the following algorithm is used:

1. For each I x I pixel sample block in the coarsest level of pyramid 1, calculate a displacement vector by finding the global maximum of the correlation with the coarsest level of Pyramid 2. Generate a confidence measure for the displacements.

2. For each finer resolution level of the pyramid do the following:

   a. Smooth the displacement vector field for the previous (coarser) pyramid level in order to remove gross errors. This helps prevent errors in the top levels of the pyramid propagating to the lower levels.

   b. Interpolate the displacement vector field calculated at the previous pyramid level to provide displacement estimates for each I x I pixel sample block of the current level of pyramid 1.

   c. For each I x I pixel sample block of the current level of Pyramid 1 find the local maximum of the correlation with the current level of Pyramid 2 by searching in an M x M window centered at the displacement estimate of the current level of Pyramid 2.

The algorithm starts at the top, coarsest pyramid level and proceeds 'top-down' one level at a time. At the coarsest level, the area to be searched in the second image is not constrained, i.e. M is the dimension of the entire image. It is very important to have valid estimates at this stage since the following stages are dependent on the first. At each successive level in the pyramid, the estimated location of the largest correlation found at the previous, coarser pyramid level constrains the locations searched. These location constraints greatly decrease the total number of locations that must be searched. The overall gain in speed over brute-force correlation is between 100 and 1000.

The selection of the size (I) of the correlation sample block involves a trade-off between accurate determination of the location of correlation maximum (small I) and avoidance of false correlation maxima (large I). Vesecky et al. (1987) describe a cross correlation technique for choosing I. The choice of I is dependent on image content. For the sea ice image of Fig. 1, an I corresponding to about a 4x4 km block size was judged to be near optimum, i.e., I = 16 for 250 m size pixels. This size is of the order of the size of the average ice floe.

The quantity M is selected to correspond to a search area of the order of the physical size of the correlation sample block in the coarser pyramid level just processed. We have taken M such that the search area is 4 times larger than the previous (coarser) level sample block size. Further information on the IPAC method is

given by Fily and Rothrock (1986), Vesecky, et al. (1986, 1987 & 1988) and Samadani (1987).

B. Confidence Estimates

There are two parts of the pyramid algorithm where confidence measures are useful. For the final vector output, confidence measures can be used to prune or to at least highlight suspect vectors. In addition, during the interpolations from a coarser pyramid level to a finer pyramid level, the confidence measures can be used as a weighting factor for the interpolation (Mostafavi and Smith,1978). The first technique was used in obtaining the results of Fig. 2. It is shown by Vesecky et al. (1988) that there is a correspondence between areas of low confidence and errors in the displacement field estimated by the IPAC method.

C. Smoothing Techniques

In the "real" world of sea ice remote sensing using SAR images one encounters noise, grey level variation across a given image and between images as well as gross geometric distortions. These problems result in errors when block correlation is used for finding ice displacement vectors. In view of these problems, the assumption is usually made that the displacement field is smooth for most areas of the image (Borodachev,1984). Smoothing techniques may be used to remove the gross errors in the displacement field. These techniques are especially important for pyramid correlation because errors made at the coarser resolutions propagate to the finer levels due to the constraints on search locations at the finer levels. One must be careful when using smoothing techniques, however, in areas where there is high shear.

In the algorithm described in section II.A above, smoothing of the estimated ice velocity field was done at each pyramid level by the following procedure. The coarse level vectors were replaced by the median of the surrounding high confidence vectors. Bilinear interpolation was then used to fill in vectors for the next higher resolution level in the pyramid. At the highest resolution level of the pyramid this procedure produced a preliminary result leading to Fig. 2.

To achieve the result of Fig. 2 we applied a different smoothing technique to the preliminary result above by extending the controlled-continuity splines method of Terzopoulos (1985) for fitting vector fields. This more versatile interpolation technique makes systematic use of the confidence measure and minimizes the weighted square deviation from the displacement data while at the same time minimizing the integral of the second spatial derivatives. Samadani (1986) gives further discussion of this smoothing technique.

D. Results for SEASAT SAR Image Pair

The pyramid algorithm described above was applied to two averaged (250 meter pixels) SEASAT images of central arctic pack sea ice - Rev. 1439 (October 5, 1978) and Rev. 1482 (October 8, 1978), Fig. 1, by Vesecky et al. (1986 & 1988). Fig. 2 compares these displacement vectors with a computer assisted manual analysis by Thorndike and Rothrock [see Weller et al., 1983]; it is seen that the method performs

very well. However, there are areas where the automated algorithm has generated erroneous velocity vectors. The problem areas at the edges of the figure correspond to ice features flowing into or out of the finite area of these images. Further discussion of errors is included in section V. The results of Fig. 2 can be used to calculate the divergence and curl of the velocity vector field as done by Vesecky et al. (1988). These fields in turn can be used to investigate sources, sinks and vorticity in the ice flow as well as appearance and disappearance of open water.

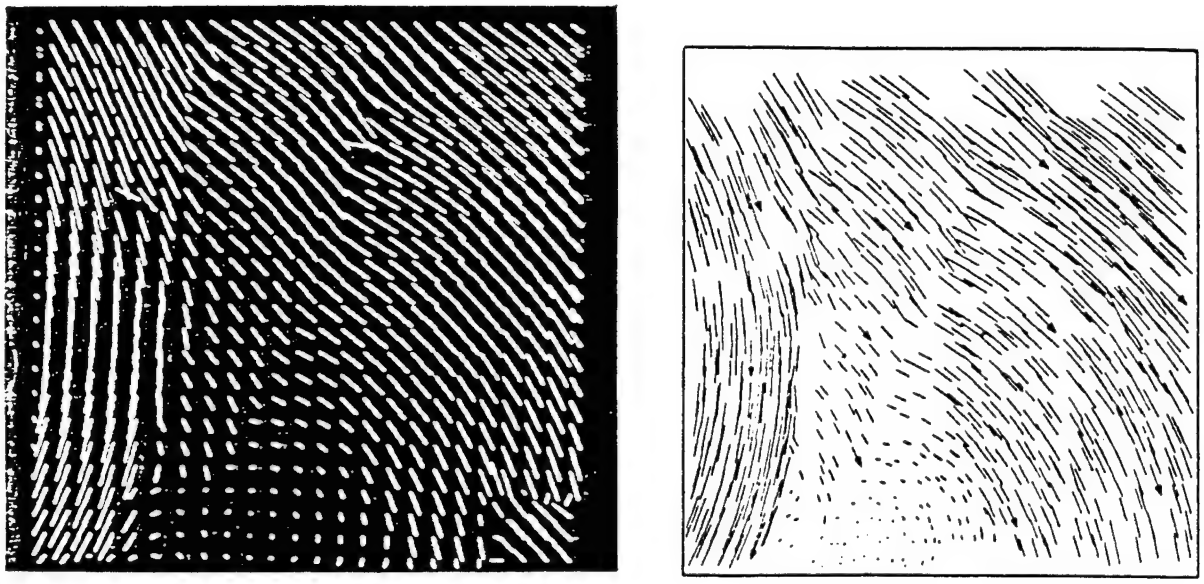

Fig 2. (left) Sea ice velocity vectors generated by the image pyramid area correlation technique (IPAC) applied to the SAR images of Fig. 1, (right) sea ice velocity vectors generated from the same image data of Fig. 1 by Thorndike and Rothrock using a computer assisted manual technique. The IPAC velocity estimates above have been improved by pruning of low confidence estimates and using the controlled-continuity spline technique for interpolation.

III. FEATURE TRACKING

A. Introduction to the Method

Feature tracking approaches the problem of sea ice motion estimates somewhat differently by relying on selected sea ice features rather than the content of the entire image. There are a wide variety of features in sea ice which one could track, including pressure ridges, isolated floes and floe-lead boundaries. The results of Fig. 3 below rely on floe-lead boundaries as the physical feature to be tracked because they are usually the most prominent, distinct and high contrast features in SAR images of sea

ice. The movement of these features from one image to the next provides the 'tie points' from which the sea ice velocity field is estimated. Feature patterns must be very distinctive, if not unique, objects. They are characterized by information which is independent of the object location and orientation, though this latter information is, of course, attached to them. The collection of several hundred features, each described by several hundred numbers, reduces the information needed to characterize a 100 x 100 km SAR image by roughly two orders of magnitude. The search space is correspondingly reduced.

Once a feature pattern is recognized in both members of a pair of images, sea ice displacement and hence velocity information can be derived. Since we know the movement of every pixel in the feature, we can derive not just one, but many velocity vectors. Further, we know the rotation as well as the displacement of a feature, since we keep track of a feature's geographic orientation in both images of the pair. The results shown in Fig. 3 below are for floe-lead boundaries; however the method can also be applied to other features such as pressure ridges or isolated floes.

B. Description of a Feature Tracking Algorithm

Here we briefly describe the feature tracking algorithm of Vesecky et al. (1988) which uses floe-lead boundaries as the features to be tracked. Each of the pair of SAR images is first averaged to a resolution of about 250 m. Ice and lead are then classified by a simple intensity threshold and floe-lead boundaries identified. Pixels along floe-lead boundaries are classified and assembled into segments. These boundary segments are characterized and thus form the features which are tracked from one SAR image to another collected three days later. Several tracking passes are made through the collections of features in each image. The high confidence ice displacement estimates, corresponding to high correlation between the characteristics of matching features in the two images, are used to guide the search for other matching features and thus more ice displacement estimates.

First, both SAR images of a pair are averaged to increase the pixel size from the original 25x25 m size to 250x250 m size. Averaging reduces the speckle variance inherent in SAR images and make computation more tractable since there are a factor of 100 fewer pixels to deal with after averaging. Since SAR pixels cannot be located geographically to better than about 200 m, the averaging process results in little loss of velocity measurement accuracy.

A histogram of pixel intensity is formed and a simple pixel intensity threshold chosen to distinguish between ice floes and leads. Fily and Rothrock (1986) have shown that this technique is viable for central pack ice. Thus the SAR image pair can be transformed into a pair of images with binary pixels, i.e. 1 for ice floe pixels and 0 for lead water pixels (including new ice). Floe-lead boundary pixels are identified simply by finding water pixels adjacent to ice pixels.

Next, the ice-water boundary pixels identified above are classified into eight types according to their surroundings to determine the orientation of the floe-lead boundary edge. The four nearest neighbor pixels are considered to find if there is water above, below, to right or to left of a given boundary pixel. The classified pixels are then

assembled into boundary segments which are the features to be tracked. The assembly scheme begins by finding the dominant boundary direction. In Fig. 1 the dominant direction is vertical, so the boundary segments are divided into two groups, corresponding to left and right edges of the leads in Fig. 1.

The goal, then, would be to match left edges in one image with left edges in the other image and, independently, right edges in the two images. This allows the ice floes along the left side of a lead to slip with respect to ice floes along the right side. Thus shear motion, which we would expect across leads in central pack ice, is built into the algorithm for this type of sea ice.

Boundary segment features are characterized by their deviation from a straight line. First, a 'least squares' criterion straight line is fit to a given boundary segment assembled as above. The distance from this straight line to the segment is calculated at regular intervals along the straight line. This set of deviations characterizes the shape of a boundary segment. Note that this method of characterizing a boundary segment feature is invariant under rotation of the feature.

Recognition of matching features is done simply by comparing the sets of deviation measurements for two candidate features. A variance normalized, cross-correlation coefficient (C) was used to evaluate how closely two candidate features matched. Often segments which we want to compare are of different lengths because of partial breakup of a boundary segment over the three days between images. So in the search, features of different lengths were included. During the comparison process the shorter features slide along the longer features with C calculated for all placements of the smaller feature with respect to the larger. This allows for larger segments to break into smaller ones and still be found.

The search and matching procedure is an iterative one and has features which remind one of the image pyramid method of section II above. During the several iterations of the search we use the high confidence ice displacement estimates of the initial iterations to guide the searches of subsequent iterations. In the first iteration only long boundary segments are used since the larger number of pixels gives a more stable estimate of C and a correct match yields ice displacement estimates over a larger region. The search is limited to a displacement of 60 km--20 km per day for the three days between the images. This search area could be significantly reduced if environmental data such as local winds were available to indicate probable ice movement.

C. Results for SEASAT SAR Image Pair in the Beaufort Sea

Fig. 3 shows the results of applying the boundary segment feature tracking algorithm to the pair of sea ice images shown in Fig. 1. Only the highest resolution, 250x250 m pixel size, images are used. Boundary segments constructed from these images vary in length from 4 to 163 pixels or 1 to 41 km in length and have a dominant direction which is vertical, i.e. North-South, in Fig. 1. The resulting sets of boundary segment features in the reference (first in time) and test (second in time) images are shown in left and middle panels of Fig. 3.

In the initial iteration only the longer segments of image 1439 with lengths greater than 30 pixels (7.5 km) were considered. Thus in the test image (orbit 1482) matching segments of length n/2 = 15 pixels and above were considered in the search. The rather strict criteria on matching features were successful in removing many erroneous matches, although it did also eliminate a few correct matches as well. The subsequent iterations added progressively fewer matches until by the seventh iteration no new matches were found. The primary difficulty lies in making sure incorrect matches are rejected rather than making sure correct matches are retained.

The right panel of Fig. 3 shows the resulting ice displacement vectors for the image pair of Fig. 1. These displacement vectors agree very well with the manually generated and IPAC displacement vectors of Fig. 2. We note that there are large regions where no displacement vectors are shown. This situation arises from two causes. First, no ice displacement vectors will be generated in regions where there are no lead-floe boundary features to be tracked. The second is that in regions where there is too much deformation a boundary segment in the reference image will often be too badly broken up in the test image to be recognized. In the first case other features, such as pressure ridge patterns, could be tracked as well as the lead-floe boundary segments. In the second case the use of higher resolution images might be helpful if the deformation were less severe at smaller size scales. A drawback of using higher resolution pixels in SAR images is that speckle noise becomes a significant component of the intensity variation from one pixel to the next.

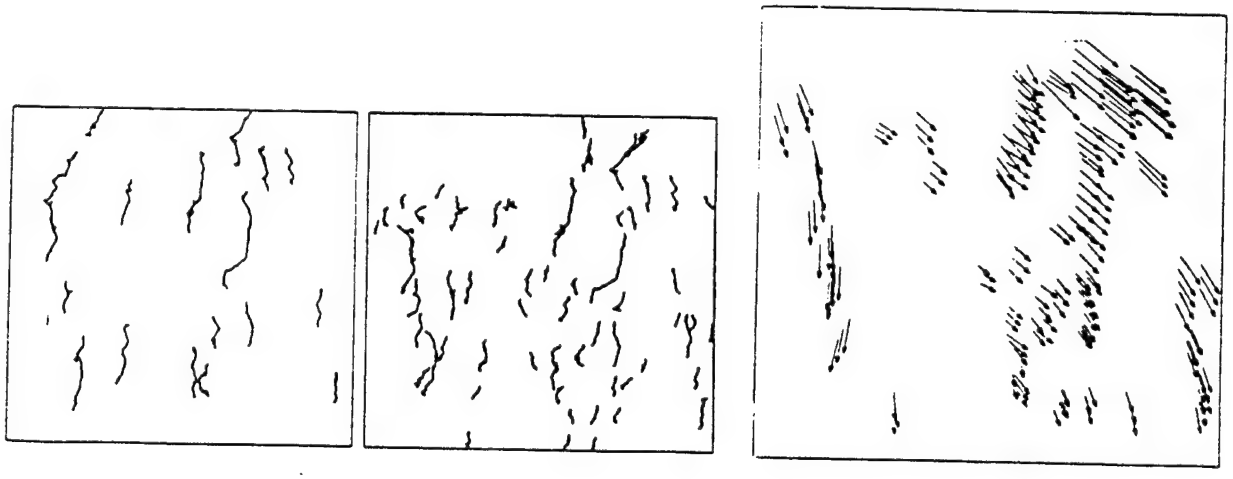

Fig. 3. Search spaces of long floe-lead boundary segments for the reference (orbit 1439) image (left) and test (orbit 1481) image are shown in the left and middle panels respectively. The right panel shows ice velocity estimates obtained by applying the boundary segment feature tracking algorithm to Fig. 1 images.

IV. TRACKING SEA ICE WHICH ROTATES

The automated ice tracking algorithms above work reasonably well in regions where there is little rotation and distortion, e.g. in portions of central pack ice (Fily and Rothrock, 1986 and Vesecky, et al., 1988). However in regions where there is significant ice rotation, > 10° to 15°, the existing image pyramid area correlation (hierarchical correlation) methods are not expected to work well because the cross correlation comparisons are made between image blocks which have been translated in position, but not rotated. For the image pair of Fig. 1, upon which the image pyramid algorithm works well, the maximum ice rotation is some 5°. As noted in section V, ice motion containing shear and distortion can also cause errors when using IPAC.

A. Block Correlation Function in the Presence of Rotation and Shear

We have studied the effect of rotation and shear on block correlation by simulating distortions on the computer. We are able to remap an image by specifying any linear transformation between the coordinates of the original image and the output image and then using bicubic interpolation to resample the image. In particular, we can simulate rotation and pure shear using the following matrices:

Rotation:

$$\begin{pmatrix} \cos\theta & -\sin\theta \\ \sin\theta & \cos\theta \end{pmatrix}$$

Shear:

$$\begin{pmatrix} 1 & -\tan\theta \\ 0 & 1 \end{pmatrix}$$

Using the remapped images the two-dimensional correlation function for typical SAR sea ice scenes can be calculated under ice rotation or shear according to the matricies above. For no rotation or shear, $\theta = 0$, the correlation function is unity and no problems occur. As θ increases, the correlation decreases and the probability of a mismatch becomes significant. That is, when we compare a scene with itself we expect unity correlation coefficient; but we don't get it if rotation or shear has distorted the scene we are comparing with our reference scene. One could, of course, persue block correlation with both translation **and rotation.** However, compution time would increase by a factor of about 10 to 100.

Vesecky et al. (1987) used two 100x100 km SAR images of pack ice from SEASAT orbits 1439 and 1396 to study the autocorrelation of sea ice scenes under rotation and shear. This experimental study consisted of extracting twenty non-overlapping 16x16 subimages at 125 meter pixels and applying both the above transformations to each subimage at increments of one degree. The correlation coefficient between the original and the rotated or sheared image was then calculated for a window size of 16x16 pixels, as used in the IPAC algorithm of section II. Fig. 4 shows a plot of the average

correlation coefficient for the twenty subimages as a function of angle of rotation or angle of shear, θ.

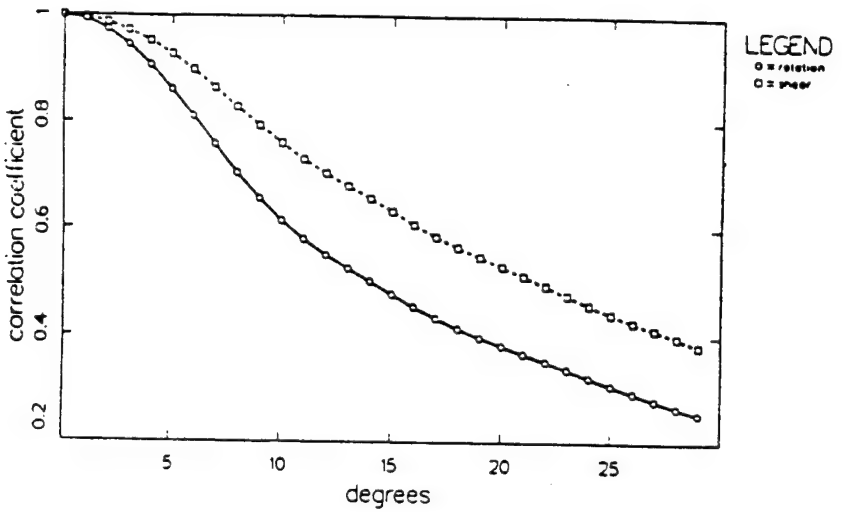

Fig. 4. Effects of rotation and shear on correlation coefficient. Averaged two-dimensional cross-correlation function with respect to angle of rotation and angle of shear (θ).

If the correlation coefficient of the correct match is low, then the probability of a mismatch increases. In one case, when we searched a local area around the correct match, we found a higher correlation coefficient than the correct one when the rotation angle was 16 degrees. The maximum correlation coefficient was .39 and the distance to the correct match was about 3 pixels. We believe that rotations of 10° or less will not hamper detection by block correlation.

One can intuitively interpret the fact that the shear curve lies above the rotation curved by considering the overlap of pixels for a given shear or rotation. The pixels in the middle row of the image are fixed for a shear whereas only the middle pixel is fixed for a rotation.

In summary, the IPAC method of section II is strictly valid only for translational motion. However, ice motion is not always pure translation, but has rotational and nonuniform translational components. Studies of simulations of rotations and shears, Fig. 4 and Vesecky et al. (1987), have shown that IPAC is still useful, up to moderate angles of distortion. In particular, we believe that rotations of up to about10° can be dealt with adequately with correlation.

B. Rotation Invarient Correlation

Invariant moments are a pattern recognition technique used to help solve the problem of identifying objects in a scene that changes because the objects translate or

rotate from one image of the scene to the next. As mentioned above, IPAC will handle rotations in sea ice features up to about 10°. Beyond that, rotations will start to affect the ability of the algorithm to correctly track features. Rotations of that magnitude or greater commonly occur in places such as the marginal ice zone. One way to work around these large rotations is to use a method that ignores rotations in a scene altogether. Invariant moments is one such method, whereby invariant moments reduce a scene to a set of numbers, indices that do not change with rotation. We think that invariant moments may also help sort out ambiguities which occur with IPAC algorithms applied to regions of pack ice that undergo rotations greater than the limits suggested above.

However, the problem of matching sea ice features is more complex than simply the problem of coping with rotational transformations because sea ice features may change with translation or rotation as ice floes move across open water or ice fields. Floes may collide with each other, thereby creating new features. Rotation of floes can affect how features are manifested in a SAR image because of changes in aspect angle (Carsey et al., 1983; Curlander et al., 1987). Translations of floes might occur across a changing background of new ice, wind-roughened ocean or pack ice. A sea ice tracking algorithm is put to task under these conditions.

Although a variety of rotation-translation invariant measures exist, we use those given by Hu (1962). These seven indices demonstrate invariance under translation and rotation. Furthermore, they also demonstrate invariance under scaling and optical inversion. Such properties — invariance under translation, rotation, scaling, and optical inversion — make these indices well suited for scene matching problems (Wong and Hall, 1978). To show why Hu's invariant moments have these properties, we will highlight their derivation.

Hu's invariant moments start with the theorem stated by Papoulis (1965). In essence, this theorem states that a scene, over the (x,y) plane with an image intensity function I(x,y), can be represented by a unique sequence of double moments m_{pq}. These moments m_{pq} are integrals over the scene with integrands of the form $x^p y^q I(x,y)$. This means that an image containing many thousands of pixels large can be compressed to a sequence of a few numbers, e.g. Hu's invariant moments. Note that low-order double moments of images are analogous to moments for objects (mass, center of mass, moments of inertia).

Double moments by themselves show no invariant properties. However, Hu derived invariant moments from double moments with a series of transformations. From double moments, we obtain central moments. Under the translation of coordinates, central moments remain invariant. From central moments, we obtain normalized central moments. Under scaling, in addition to translation, normalized central moments remain invariant. From normalized central moments and with the theory of algebraic invariants, we obtain Hu's indices. Under proper and improper orthogonal rotation and mirroring, in addition to translation and scaling, Hu's indices remain invariant. Finally, since the magnitude of these moments may span many orders, the typical convention is to take the absolute value of the log of Hu's indices.

Vesecky et al. (1987) have applied Hu's invarient moments to rotating ice floes in the marginal ice zone. Ice floes which have rotated 90° and more are correctly identified even though they have changed appearance somewhat due to the aspect angle dependence of SAR images. However, false matches were also encountered. Rotational invarient correlation methods are subject to limitations imposed by the discrete nature of digital images, changes in the background against which the floe is imaged (e.g. surrounding floes), aspect angle dependence of SAR images and changes in the tracked floe itself (e.g. bits breaking off). In spite of these limitations we think that rotation invarient correlation will fine useful application in tracking sea ice which rotates. The essential items for successful application of rotation invarient correlation appear to be isolating a tracked floe from its background and finding an effective similarity measure between the invarient moments of two floes.

C. Feature Tracking

The feature tracking algorithm is inherently robust with respect to rotation because the features are characterized with respect to a coordinate system tied to the feature itself and not with respect to geographic or image coordinates. To understand this we consider the characterization process in more detail. After pixels along floe-lead boundaries are classified and assembled into segments these boundary segment features are characterized by their deviation from a straight line. First, a 'least squares' criterion straight line is fit to a given boundary segment. The perpendicular distance from this straight line to the segment is calculated at regular intervals along the straight line. This set of deviations characterizes the shape of a boundary segment. Recognition of matching features is done simply by comparing the sets of deviation measurements for two candidate features. A successful match reveals ice motion.

Because this method of characterizing a boundary segment feature is invariant under rotation of the feature one expects that, in principle, a feature which has undergone rotation will be as easily found as one which has not. In the one pair of SAR sea ice images so far examined by Vesecky et al. (1988) features were successfully tracked using this algorithm (Fig. 3). However, the SAR scenes contained central pack ice and the average rotation of the sea ice was only about 5°.

Although our feature tracking algorithm has advantages in terms of following rotating ice, there are also limitations so far as the algorithm of section III is concerned. The limitation arises, not in the characterization of a feature, but in choosing what pixels constitute the feature. Features are constructed by first classifying floe-lead boundary pixels and then assembling them into contiguous sequences of pixels having only certain allowed classifications. The classification system uses surrounding pixels for reference and thus is not completely independent of image coordinates. This process allows two sides of a lead to be separate features and thus move independently, i.e. it allows leads to open and close. Thus the lead-floe boundary surrounding a lead may be chopped into features (for tracking) in two different ways depending on how it is oriented in the first and second images of an image pair.

Feature tracking is a broad catagory of pattern recognition techniques for application to sea ice. It has inherent advantages for ice tracking in the presence of rotation. The particular algorithm of section III relys on lead-floe boundaries as features and thus has limitations which arises from the fact that leads often open and close and thus the dominant edges must be tracked independently. Other sea ice features do not have this limitation. For example, pressure ridge patterns are an evident feature in Fig. 1 above. Although pressure ridges are less distinct features than lead-floe boundaries, they are more stable since they are not affected by opening and closing of leads. Thus one expects that incorporating pressure ridge patterns into a feature tracking algorithm would improve performance, particularly for large and spatially variable ice rotation.

V. IMAGE RECONSTRUCTION & SUBTRACTION for ERROR ASSESSMENT

A. Image Restoration, Remapping and Image Subtraction

The goal of this research is to produce ice velocity data for sea ice science and applications. To make the ice velocity field estimates of Figs. 2 and 3 truly useful they must be accompanied by some measure of the quality of the estimates. We have found image remapping to be a useful technique for evaluating the quality of a velocity field. The estimated ice velocity field defines a mapping between the pair of images. One can use this mapping to remap the intensities in the second image to the locations they would be found in the first image. It can be shown that the difference between the first image and the remapped version of the second image bounds the errors in the motion if there is detail in the image. Intuitively, if the motion algorithm is correct, the remapped intensities subtract perfectly from the original intensities leaving zero remainder. Where there are velocity errors, the intensities will not subtract perfectly and the errors will be displayed as bright portions in the difference image.

We recognize that in the practical world of SAR remote sensing there are likely to be changes in intensity between the two images in a pair which are unrelated to ice motion. For example changes in system gain, incidence angle, aspect angle and surface conditions (such as snow and wind) can cause variations in SAR image intensity. However, the successful results of Fig. 5 below resulted from the pair of SEASAT SAR images shown in Fig. 1. So we are optimistic that the method will have application to a significant fraction of satellite SAR observations of sea ice, which are less subject to the variations mentioned above than aircraft observations.

B. Error Detection by Image Subtraction

Fig. 5 shows the absolute value of the difference between the 5 Oct. (orbit 1439) image and the remapped 8 Oct. (orbit 1482) image of Fig. 1. The remapped 8 Oct. image was created using the smoothed IPAC velocity vector estimates of Fig. 2. The difference picture has been displayed so that image intensity differences greater than a chosen threshold value are bright and those below are dark. Thus high error regions are bright and low error regions are dark.

This image provides a convenient display of the regions where the ice velocity estimates are likely to be in error. Here we have assumed that the ice itself remains the same, as seen by the SAR, in the two images. This error map can be used in two ways. First, it can be used as a guide to the credibility of the ice velocity field estimates provided by SAR. Thus the ice science or applications user is in a position to know when and where the ice velocity data provided to him are dependable or likely to be in error. Second, the error data can be used as feedback within an ice velocity estimation algorithm to improve the velocity estimates.

Fig. 5. Image reconstruction and subtraction map based on the ice velocity field of Fig. 2. Regions where the ice velocity estimates are likely to be in error are bright and low error regions are dark.

C. Interpretation of Image Subtraction Results

By comparing the error display of Fig. 5 with the ice velocity field as shown in Fig. 2 we find that we can make an interesting interpretation of the error display. First, we note that the large dark areas where errors are low correspond to large blocks of ice which move as rigid plates. These large units were also pointed out by Fily and Rothrock (1986). Second, we see that the large error (bright) regions tend to fall along lines which separate the large rigid plates. It is in these regions that the large plates apparently grind against one another producing velocity shear which deforms the ice. The deformation of the ice in these regions, coupled with the fact that the ice velocity estimates are discrete and smoothed, causes errors in ice velocity estimates. Thus we suggest that the remapping error plots such as that shown in Fig. 5 can be used to segment an ice velocity field into dark regions which tend to be large rigidly rotating plates and bright regions where there is much shear and ice deformation.

VI. SYNTHESIS of a GENERAL SEA ICE TRACKING ALGORITHM

In work described here as well as that by Fily and Rothrock (1986), Michael Collins (1987), Tom Hiroshi and others we find several schemes for automated sea ice tracking and the estimation of sea ice velocity fields. At this stage it appears that the different algorithms each have their own relative advantages and disadvantages. The relative advantages of IPAC and feature tracking have been discussed by Vesecky et al. (1988). No one algorithm is clearly superior over a wide range of sea ice conditions. Thus it appears that a synthesis of several methods will be most likely to provide a robust, automated sea ice tracking algorithm.

To illustrate the roles of various methods we briefly describe several techniques and where they might fit in an algorithm synthesis. Collins (1987) has shown that a matched filter approach implies that the image data should be filtered before any correlation algorithms are applied. The resulting 'high pass' filter would emphasize the edges in the images and make correlation work more effectively. Before IPAC or related block correlation techniques can be applied the amount of ice rotation shoule be assessed and compensated for if greater than about 10°. Feature tracking and rotation invarient correlation could be used to estimate ice rotation (so that it could be compensated for in an IPAC scheme) or provide alternatives to block correlation techniques. The point here is that the different ice tracking methods can be used to mitigate the deficiencies in one another.

On way of thinking about the structure of a synthesis algorithm is to consider series and parallel strategies. In a series strategy the various component algorithms would be applied in sequence. An example of this type of algorithm was presented by Curlander (1987). The idea is to use a feature tracking algorithm first to define the gross ice motion, including rotation, if any. This preliminary estimate of the velocity field would then be used as a basis for application of an IPAC type technique. At each location where block correlation is to be carried out the scene in the test image (second in time) would be counterrotated according to the rotation estimate of the first step so that block correlation would effective as discussed in section IV above.

An example of a parallel structure is shown in Fig. 6 (Vesecky, 1987). Here IPAC is the primary technique with feature tracking and rotation invarient correlation being employed to check consistency and in locations where IPAC yields low confidence estimates. Referring to Fig. 6 we see that environmental data, primarily surface winds, are used to select the pair of SAR scenes which are the input to the tracking algorithms. Feature tracking is used as subordinate technique to confirm or disagree with the IPAC estimates. At each level in the pyramid the ice velocity field estimated by IPAC is checked for confidence (as discussed in section II.B) and consistency with the feature tracking (discussed in section III) velocity estimates. Rotation invarient correlation methods could come into play here to revise IPAC velocity estimates which are either low confidence or inconsistent with feature tracking estimates. Velocity estimates which remain below a confidence and consistancy threshold are then removed and a substitute generated by interpolation from surrounding velocity vectors (see section II.C). After the lowest level in the IPAC pyramid has been completed error estimates are

computed by using the image reconstruction-subtraction scheme (section V). After an unspecified last effort to resolve vectors which are likely to be in error the system produces its output, namely: V(x,y), sea ice velocity estimates as a function of time and geographic position (Figs. 2 and 3) and error estimates for V(x,y) as shown in Fig. 5.

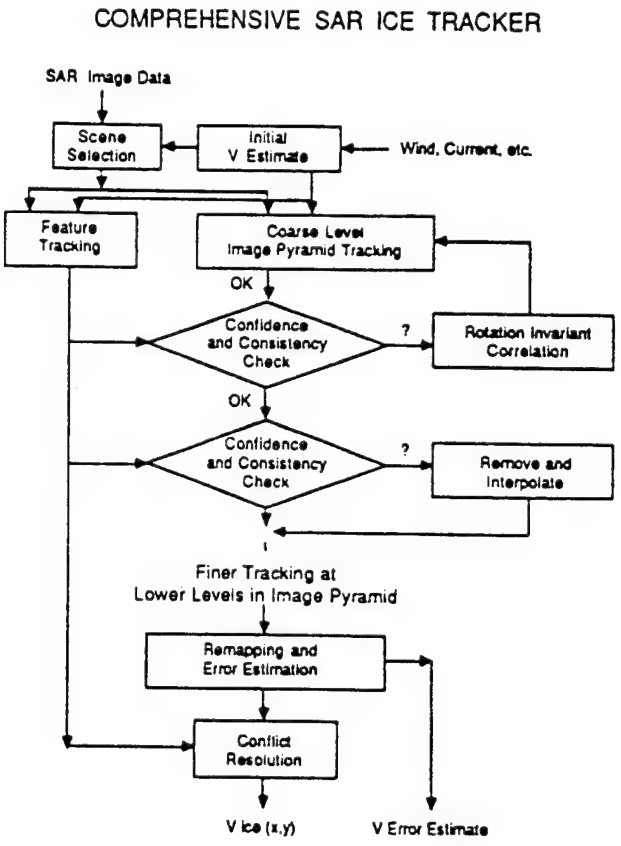

Fig. 6. Schematic block diagram for a comprehensive automated system for estimating sea ice velocity from SAR images. This scheme incorperates several techniques by using a parallel algorithm structure.

VII. DISPLAY OF SEA ICE VELOCITY DATA

While accurate ice velocity estimates are most important, effective display of the results to the user is a vital link in using SAR images in sea ice science and applications. For it is the user who will interpret the ice velocity fields. An ineffective display scheme can not only foil creative interpretation by producing artifacts in the display, but can also obscure significant features.

As an example, consider the commonly used line or arrow display of Figs. 2 and 3. While this display seems perfectly adequate, note that artifacts which draw the eye are

produced when the lines happen to be horizontal, vertical or inclined at 45°, i.e. when the arrow heads follow the tails of their neighbors. Clearly this artifact is related to the choice of coordinates and has no physical significance in ice science.

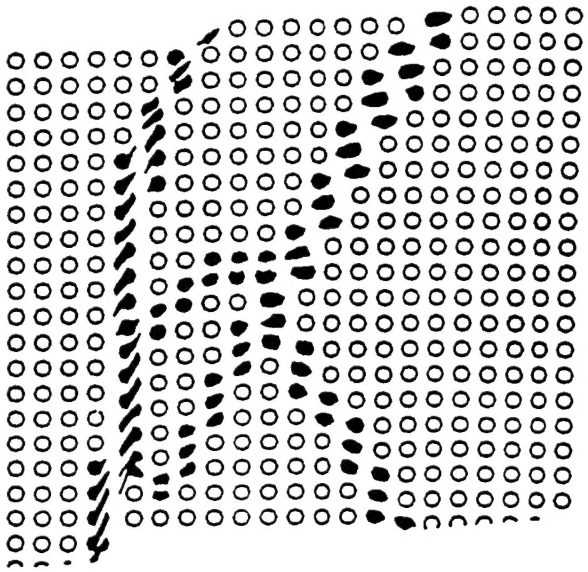

Fig. 7. Hexagon display scheme for emphasizing shear and distortion in a sea ice velocity field.

Other types of displays are possible and we think can contribute significantly to the interpretation of sea ice velocity data. For example, suppose that one wants to emphasize the distortion or shear in an ice velocity field. The scheme illustrated in Fig. 7 uses a pattern of octagons placed on the original SAR image at regular intervals. The ice velocity field is then allowed to move each vertex of each octagon. If the ice velocity field is uniform, an octagon retains is shape. If there is velocity shear or other distortion, then each octagon distorts accordingly. The velocity field used to construct Fig. 7 is that of Fig. 2. We have darkened the hexagons which are distorted to emphasize regions of shear and distortion. Note the correspondence between Figs. 5 and 7 which both make clear the large, rigidly moving plates of ice and the regions of shear and distortion between them, where they grind together.

VIII. CONCLUSIONS

1. The image pyramid area correlation algorithm (IPAC) provides a useful, though not ideal, means of automating the process of deriving sea ice velocity information from SAR images.

2. Feature tracking using floe-lead boundary segments produces sea ice velocity estimates which agree well with IPAC and manual results, but are limited to regions where features are found. Extension to pressure ridges and other features is indicated.

3. Current block correlation schemes are likely to be in error when ice rotation is >

10° between images. Feature tracking and rotational invarient correlation can provide tracking capability when the ice rotates.

4. Image reconstruction and subtraction provides a convenient measure of regions where ice velocity estimates are likely to be in error.

5. A robust, automated sea ice tracking algorithm will need a variety of techniques to operate successfully over a wide range of sea ice conditions. A synthesis of several available techniques is indicated.

6. Effective display of sea ice velocity information is important for effective interpretation of the data.

ACKNOWLEDGEMENTS

We are grateful to Frank Carsey, John Curlander and Ben Holt at the NASA Jet Propulsion Laboratory for supplying sea ice SAR images. Sieglinde Barsch and Stephen Vesecky are acknowledged with thanks for their help in manuscript and figure preparation. We gratefully acknowledge guidance, encouragement and financial support from NASA Oceanic Processes (Ken Jezek and Robert Thomas) and the Office of Naval Research, Code 1125RS (Charles Luther). We also acknowledge with thanks NASA financial support via the Center for Aeronautics and Space Information Systems, Stanford EECS, NASA grant NAGW 419.

REFERENCES

Borodachev, V. E., The block structure of the ice cover, in **Dynamics of Ice Cover** (L. A. Timokhov, ed.), Oxonian Press, New Delhi (1984).

Carsey, F., J. Curlander, B. Holt and K. Hussey, Shear Zone Ice Deformation Using Supervised Analysis on SEASAT Data, **A.I.A.A. 21st Aero. Sci. Meet.,** Reno (1983).

Collins, M. J., Ph. D. Thesis, University of British Columbia, Vancouver, B.C. (1987).

Curlander, J., Presentation to Ice Motion Working Group, Jet Propulsion Laboratory, Pasadena, Sept. (1987).

Curlander, J., B. Holt and K. Hussey, Determination of Sea Ice Motion Using Digital SAR Imagery, **I.E.E.E. J. Ocean Engr.,** in press, (1987).

Fily, M. and D. A. Rothrock, Extracting Sea Ice Data from Satellite SAR Imagery," **IEEE Trans. Geosci. & Remote Sensing, GE-24**, 849-854, (1986).

Hu, M-K., Visual pattern recognition by moment invariants, **IRE Trans. Infor. Th.**, 8,179-187 (1962).

Mostafavi, H. and F. Smith, Image correlation with geometric distrotion. Part 1: acquisition and performance, **IEEE TRans. Aerosp. Electronic Sys., AES-14,** 3 (1978).

Samadani, R., "Image Pyramid Motion Detection Applied to Sea Ice", Rpt. D303-1987-1, STAR Laboratory, Elec. Engr. Dept., Stanford University, Stanford CA (1987).

Terzopoulos, D., Computing visible-surface representations, MIT Artificial Intelligence Lab., Memo 800 (1985).

Vesecky, J. F., Presentation to Sea Ice Motion Working Group, ERIM, Ann Arbor MI, May (1987).

Vesecky, J., R. Samadani, M. P. Smith, J. M. Daida and R. N. Bracewell, Automated remote sensing of sea ice using synthetic aperture radar, **Proc. IGARSS'86**, 127-132, ESA SP-254, ESA Publ. Div., Paris (1986).

Vesecky, J., R. Samadani, M. Smith, J. M. Daida and R. N. Bracewell, "Observing Rotation and Deformation of Sea Ice with SAR, **Proc. IGARSS '87 Conf.**, 1137-1145 (1987).

Vesecky, J., R. Samadani, M. Smith, J. Daida & R. N. Bracewell, Observation of sea ice dynamics using synthetic aperture radar images: automated analysis, **IEEE J. Geosci. & Rem. Sensing, GE-26**, 1, 38-48 (1988).

Weller, G., F. Carsey, B. Holt, D. A. Rothrock and W. F. Weeks, "Science Program for an Imaging Radar Receiving Station in Alaska -- Report of the Science Working Group", NASA - Jet Propulsion Lab. (1983).

Wong, R. & E. Hall, Scene matching with invariant moments, **Comp. Gr. & Image Proces.**, 8, 16-24 (1978).

REMOTE SENSING OF SEA ICE MOTION USING FLOE EDGE AND PRESSURE RIDGE FEATURES IN SAR IMAGES

J F Vesecky, R Samadani, M P Smith & J M Daida & R N Bracewell

STAR Laboratory, Electrical Engineering Dept., Stanford University
233 Durand Building, Stanford CA 94305-4055 USA
Tel: 415-723-2669 Telex 348402 Stanford - STNU

Synthetic aperture radar (SAR) provides an excellent means of observing the movement and distortion of sea ice over large temporal and spatial scales. SAR observations are not affected by clouds or lack of sunlight. The European Space Agency's ERS-1 satellite as well as others planned to follow will carry SAR's over the polar regions beginning in the early 1990's. Ground stations, such as NASA's Alaskan SAR Facility, will interpret these SAR images in terms of geophysical measurements of sea ice. A key component in utilization of SAR image data is an automated scheme for extracting the sea ice velocity field from a sequence of SAR images of the same geographical region. The process of retrieving motion information from a sequence of SAR images revolves around two principal items, namely:

1. Identifying regions in the image of a sea ice field to use as 'tie points' for ice floe tracking.
2. Finding the same tie points in subsequent images of the sequence.

Once the ice displacement is known the ice velocity can easily be calculated since the elapsed time between the SAR images is known. Two general techniques for automated sea ice tracking have emerged from recent research, namely: image pyramid area correlation (hierarchical correlation) and feature tracking. The first method uses a pyramid (variable resolution) data structure and relies on finding the maximum block correlation between areas in the two images. It performs in a computationally efficient manner when the ice being tracked rotates less than 10° to 15°. For ice which rotates more than 15° between SAR observations, such as in the marginal ice zone, the feature tracking method appears preferable. Whilst image pyramid techniques have been reported elsewhere, we focus here on feature tracking. Distinctive features are located and characterized in each image; thus converting each image from a set of pixels to a set of features. These features are then used as tie points to estimate ice motion. Since each image is converted from millions of pixels to sets of tens of features each characterized by about a hundred numbers, the computation time required to establish matching features is tractable. To observe ice motion when the ice rotates, the features must be characterized in a manner which is independent of orientation. Here we consider two types of features: floe-lead boundaries and pressure ridges. In both cases we process the SAR image data to emphasize the feature under consideration. For floe-lead boundaries the image is segmented into ice and water areas by thresholding and boundary segments identified by simply looking for ice pixels next to water pixels. Pressure ridges are emphasized by

Proceedings of IGARSS '88 Symposium, Edinburgh, Scotland, 13–16 Sept. 1988. Ref. ESA SP-284 (IEEE 88CH2497-6).
Published by ESA Publications Division, August 1988.

expanding the brighter portions of the image and thresholding. Gaps in filamentary features are filled in using a growth and erosion technique. Boundary segments are characterized by fitting a straight line to the segment and noting the deviation of the segment from this line. Pressure ridges are characterized by using a fitted line as the 'trunk' of a tree structure with branches jutting out from the trunk at different points and angles for different distances. Since these features are referenced to a line and the line can have any location and orientation, the set of numbers characterizing the feature is independent of the feature's location and orientation in the image. Once each image is converted into a set of features, the features are matched by correlation. The iterative algorithm, used in the search, looks for high confidence matches between the most distinctive features and uses these to guide further searches in terms of location. We apply these methods to several pairs of Seasat SAR images of sea ice from the Beaufort Sea and present the results. The results compare favorably with ice motion estimates made by visually finding tie points in the same images using a split screen video display.